Mapping Pine Mistletoe infestation with Very High Resolution imagery: a Sub-pixel approach

Mercy Ndalila
May, 2014

Course Title: Geo-Information Science and Earth Observation for Environmental Modelling and Management

Level: Master of Science (MSc.)

Course Duration: August 2012- June 2014

Consortium partners:

Lund University (Sweden)
University of Twente, Faculty ITC (The Netherlands)
University of Southampton (United Kingdom)
University of Warsaw (Poland)
University of Iceland (Iceland)
University of Sydney (Australia- Associate partner)

Mapping Pine Mistletoe infestation with Very High Resolution imagery: a Sub-pixel approach

by

Mercy Ndalila

Thesis submitted to the Faculty of Geo-information Science and Earth Observation, University of Twente in partial fulfilment of the requirements for the degree of Master of Science in Geo-information Science and Earth Observation for Environmental Modelling and Management

Thesis Assessment Board:

Dr. A.G. Toxopeus (Chair)
Dr. V.A Tolpekin (External Examiner, Department of Earth Observation Science, ITC)
Drs. E.H. Kloosterman (First Supervisor)
Ms. Dr. I.C. van Duren (Second Supervisor)

UNIVERSITY OF TWENTE.
FACULTY OF GEO-INFORMATION SCIENCE AND EARTH OBSERVATION

Disclaimer

This document describes work undertaken as part of a programme of study at the Faculty of Geo-information Science and Earth Observation, University of Twente. All views and opinions expressed therein remain the sole responsibility of the author, and do not necessarily represent those of the institute.

Abstract

Decline of productivity of Scots Pines due to mistletoe infestation is a serious problem in many forests in Europe. This infestation continues to cause significant economic and ecological losses within these forests. Detecting and quantifying mistletoe infestation therefore remains critical in order to prioritise areas for control and prevention measures. Remote Sensing (RS) offers an alternative and potentially more efficient means of mistletoe characterisation than field methods. However, accurate mapping with RS still remains a challenge. The scale of the mistletoe occurrence is usually much smaller than the pixel size of currently operational satellite systems. In this study, sub-pixel classification methods were adopted to assess their potential in mistletoe mapping on WorldView 2 and GeoEye 1 imagery covering Bois Noir forest, France. Specifically, Fuzzy Maximum Likelihood (FML), Linear Spectral Unmixing (LSU), Super Resolution Mapping (SRM), as well as Expectation Maximisation (EM) were tested to determine which method produced more accurate mistletoe detection. Transformed Divergence (TD) was computed to assess separability of mistletoes from other classes. Accuracy of the methods was determined through RMSE, Correlation (r) and Coefficient of Determination (R^2). From the findings, none of the sub-pixel methods yielded any tangible results, with r and R^2 of almost 0.00 obtained for all methods. RMSEs of 0.166, 0.48, 0.28 and 0.166 were obtained for FML, LSU, SRM and EM respectively. TD did not seem to play any significant role in influencing mistletoe detection, even though a high TD of 2 was obtained. Spectral confusion with other classes was therefore observed. Significantly different yet unsatisfactory results were obtained from mistletoe mapping on the two satellite images. A combination of factors might have contributed to a poor classification: a high internal variation in spectral reflectance of pine trees might have hampered mistletoes detection. In addition, insufficient and non-representative training samples for mistletoes prevented obtaining adequate pixels for mistletoe mapping. This might have contributed to possible inaccurate estimation of mistletoe statistics. Furthermore, sun elevation angle and topographic effects, poor quality of the WorldView image and geometric distortions in both images could have played a role in classification failure. Overall, mistletoe mapping in the study area was impossible. Further research should be directed towards tackling the effect of class variability on performance of sub-pixel classification algorithms. This might provide a more accurate spatial distribution of mistletoe infestation to inform long term forest management. In addition, further investigation using Unmanned Aerial Vehicles could improve mistletoe detection and mapping.

Acknowledgements

I would like to thank the European Union for granting me this wonderful opportunity to study the GEM programme in two world class universities through the Erasmus Mundus scholarship. My sincere gratitude to my supervisors Drs. Henk Kloosterman and Dr. Iris van Duren for the guidance on my thesis, your constructive criticisms and for always availing your time despite the busy schedule. Many thanks go to Dr. Valentyn Tolpekin who has been very instrumental in my work, by not only availing his programming code for this study but also for exposing me to image analysis operations I knew little about.

Dr. Yousif Hussin deserves much appreciation for availing the satellite images for this study, in addition to sharing great moments during fieldwork in France. I'm indebted to Ms. Ioulia Leventi, Mr. Nieuwenhuis and Dr. Krol for their help in aspects of this study. Thanks to Dr. Michael Weir for the academic coordination during the entire MSc. study and to Marion Pierik and Laura Windig for financial and administrative support respectively.

Learning in ITC and Lund University has opened my eyes to invaluable opportunities, skills and multicultural experiences that I'll forever treasure. I particularly thank my teachers in both universities for the academic provision and my classmates in Lund and ITC for the academic discussions, potluck dinners and trips. Aruna, Phibion, Fatemeh, Nina, Milena, Darya and Karolina, I'll miss you a lot! Thanks too to the Kenyan Community in ITC for the great gatherings.

Many thanks go to Martin for exposing me to this awesome yet competitive programme. Last but not in any way least, I thank my mum Truphena Ndalila and my siblings for believing in me and for always praying for me while I was far away from home. I miss dad and Michael. I cherish the times we spent with them.

Table of Contents

List of figures

List of tables

x

Chapter 1: Introduction

1.1 Background

The decline in productivity of Scots Pine (*Pinus sylvestris*) forest in parts of Europe has been attributed partly to the infestation of Pine Mistletoe (*Viscum. album* subsp. *Austriacum*) (Dobbertin & Rigling, 2006; Zuber, 2004). The mistletoe is a perennial, epiphytic and hemiparasitic plant known to attack pine trees by extracting water from the tree through a structure called haustorium. This swollen vascular structure serves to attach the mistletoe plant to the host tree and extracts water and minerals to the plant (Figure 1). This uptake of water from the host tree eventually affects the water balance of the tree (Sanguesa-Barreda *et al*., 2012). During drought, when the host tree closes stomata to reduce water loss, the mistletoe continues to transpire, increasing the drought stress of the tree and even inducing mortality (Fischer, 1983). Furthermore, the mistletoe takes up photosynthates and other nutrients from the host trees leading to crown degradation, loss of photosynthetic and reproductive capacity, altered resource allocation, reduced leaf nitrogen and slower growth (Dobbertin & Rigling, 2006).

Figure 1: Pine Mistletoe bush attached to Scots Pine branch (note the swollen part of the branch where the attachment forms)

The growth rate of the European mistletoe is typically not fast, taking about 5 years for the plant to develop five pairs of leaves (Figure 2). This is the time when the plant reaches reproductive stage. The plant then forms many bushes on the branches and may grow up to 27–30 years (Nierhaus-Wunderwals & Lawrenz, 1997). The main vector of mistletoe distribution is seed dispersal by birds (Roura-Pascual *et al.*, 2012; Kołodziejek *et al*., 2012). The birds which include Mistletoe Thrush (*Turdus viscivorus*), Black Cap (*Sylvia atricapilla*) and Waxwing (*Bombycilla garrula*) are attracted to the pine trees by mistletoe fruits to which they feed on. By perching on the top of trees, the birds deposit mistletoe seeds increasing incidences of spread from infected to non-infected hosts (Kołodziejek *et al*., 2012).

Vertical (gravitational) dispersal within an individual tree may also occur when seeds fall from upper crowns, stick to lower branches because of the viscin coat and germinate (Sanguesa-Barreda *et al*., 2012).

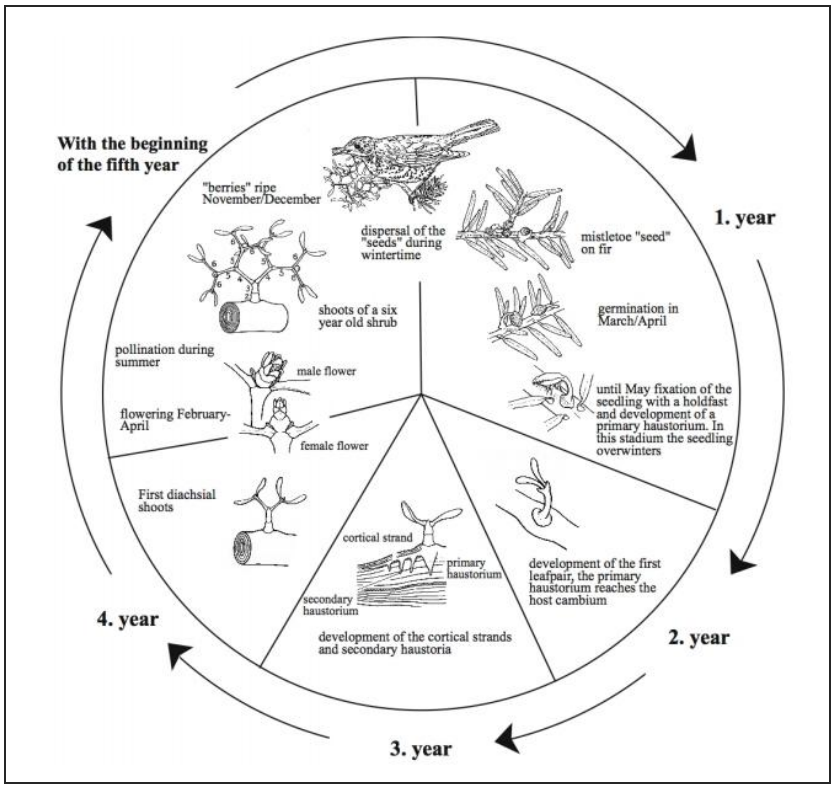

Figure 2: Life cycle of the European Mistletoe (Nierhaus-Wunderwals & Lawrenz, 1997)

Despite the slow growth rate, mistletoe distribution can be severe and when combined with other stressors such as drought, host tree mortality has been observed (Dobbertin & Rigling, 2006). In the southern French Alps and in particular Bois Noir forest, severe Pine mistletoe infestation on Scots pine forest has been reported (Chauvin & Vallauri, 2002). This has led to reduced vigour of the forest resulting in increased mortality risks of heavily infested trees (Figure 3).

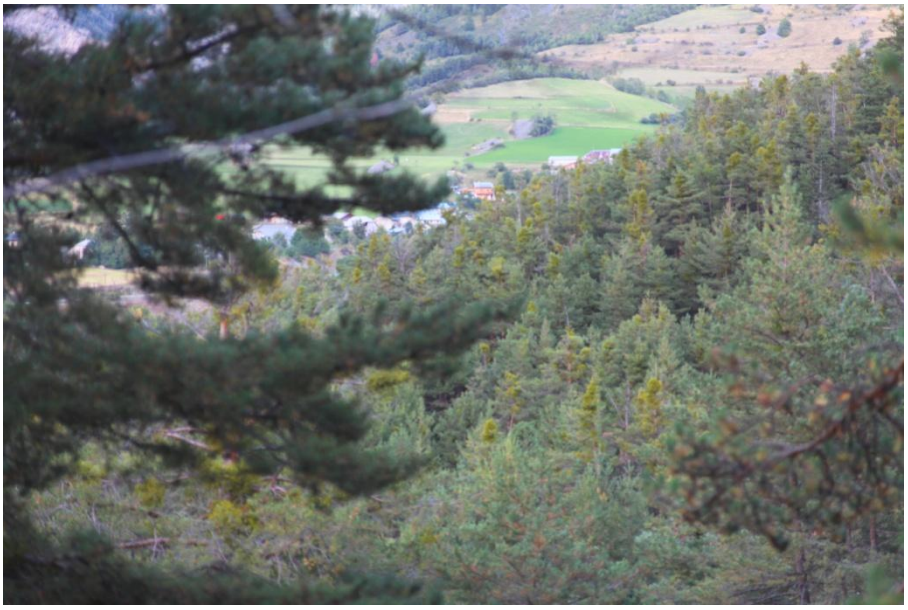

Figure 3: Heavily infested forest bordering Bois Noir forest

Pine Mistletoe distribution and Ecology

The natural distribution range of the European Mistletoe (*V. album*) to which Pine mistletoe (*V. album* subsp. *austriacum*) is a subspecies is in Europe. The Mediterranean region forms the Southern tip of its distribution while the Atlantic Ocean is the Western border. Although the habitat of Pine mistletoe is topographically and ecologically dependent on the host tree, the maximal distribution range is not the same as that of the host trees (Zuber, 2004). Temperature limits its northern and eastern distribution in Europe. The notable absence of the mistletoe in the Netherlands, Northern Germany and most of Scandinavia is an indicator that climatic conditions largely influence mistletoe occurrence (Mistletoe Matters, 2012). Though small colonies may occur in these areas, they tend to be restricted. Figure 4 shows the distribution range of the Pine Mistletoe in Europe. The plant occurs in sub-montane regions at altitudes below 1000 m, though incidentally found at higher altitudes as well.

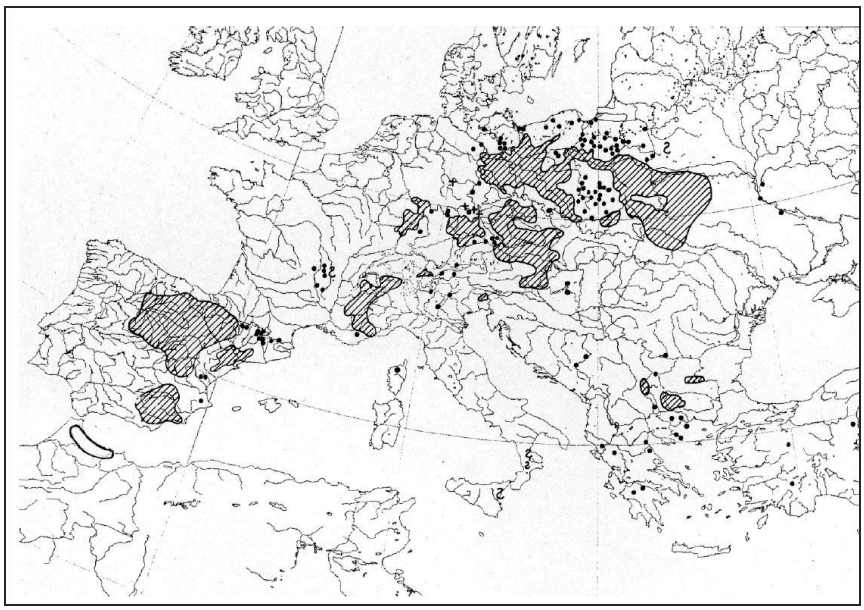

Figure 4: Distribution of Pine Mistletoe in Europe (map by E J. Jäger (Halle) in Zuber, 2004)

A variety of factors have been known to influence the distribution and growth of mistletoes in various species of *Pinus* stands. Host quality and size, landscape structure, silvicultural practice and climatic conditions are among them (Roura-Pascual *et al.*, 2012; Zuber, 2004). Pine Mistletoe is a shade-intolerant species whose growth rate increases with increasing light condition especially in more transparent tree crowns (Zuber 2004; Dobbertin & Rigling, 2006). The plant requires adequate light conditions for the mistletoe seeds to germinate and for seedlings to establish (Watson, 2001; Dobbertin & Rigling, 2006). Topography plays an important role in mistletoe distribution (McIntosh, 2004). The role is however secondary as it determines the main regulating factors such as light, temperature and moisture. Previous studies in America have shown that stands of various species of Northern America pine that occur on ridges have higher levels of dwarf mistletoe than those in valleys (Merrill *et al.,* 1987). The authors report that the mistletoe was more frequent on

the west aspects in an area in Colorado, and on the west and southwest exposures in New Mexico, United States. In another study by Dobbertin *et al*. (2005), Pine Mistletoe occurrence was reported to be higher on south- or west-facing slopes than on any other slope exposition. In addition, the authors found pines growing in the mentioned aspects were 5-28% more probable to be infested by mistletoes than trees growing on north and east-facing slopes. This may be related to the plant's strategy to access optimal areas for germination *i.e.* optimal light conditions. This also implies that areas in the landscape with favourable light conditions, in combination with the occurrence of the host species may be more liable to *V. album* infestations.

Detection of mistletoe infestation

Detection of *V. album* subsp. *austriacum* on Scots Pine forest is of great importance owing to its adverse effects relating to loss of economic and ecological functions. The pine species performs a number of functions, among them protection against soil erosion, avalanches, and rock-slides; it is a habitat and source of food for various small fauna; a source of timber; and serves recreational purposes (Dobbertin *et al*., 2005). Infestation with mistletoe has been known to suppress the growth and reduce the timber volume and overall wood quality of its host while hindering ecological integrity of the pine forest. Previous studies indicate increased vulnerability of plants infested with mistletoe to other biotic and abiotic stressors such as drought and insect attacks *e.g.* the bark beetle (Sanguesa-Barreda *et al.*, 2012; Paine & Baker, 1993). Timely detection, analysis, and reporting of adverse changes in forest health is therefore necessary to facilitate the development of decision support systems to promote forest management (Tkacz *et al*., 2008; Liang, 2004).

Detecting mistletoe infestation using traditional ecological methods, such as field studies remains a major challenge. This is because these methods are costly, time-consuming and sometimes impractical due to some areas not being accessible. Remote Sensing (RS) offers an alternative source of data that can be used to identify and map *V. album* infestations at varied spatial and temporal scales (Foody, 2000). According to Pu *et al*. (2008), the potential of multispectral RS in mapping and monitoring the degree and extent of pest infestation and species invasions has gained importance in recent years. In addition, the advancement of high spatial resolution aerial and satellite imagery and information extraction algorithms has increased the accuracy of assessment and monitoring of the health status of forests (Wierzbicki *et al.,* 2013).

Despite advances in satellite instruments and their calibration, there still exist major differences between satellites even when a target is observed at the same spatial resolution. Two examples are the WorldView 2 and GeoEye 1 satellite systems used in this study which differ in platform and sensor characteristics. One of the differences is the satellite view angle (Figure 5). Studies have shown variation of spectral response of vegetation with view angle, and the nature and extent of these variations are wavelength and cover type-dependent (Barnsley, 1984). This may ultimately affect classification results. An off-nadir field of view has been found to (1) reduce geo-location accuracy of the satellites (Satellite Imaging Corporation, 2013) as it introduces geometric distortions in areas away from nadir, and (2) increases blurring of an image when the view angle increases. Advantages of an off-nadir view are: (1) it enables wide coverage of an area being imaged, and (2) it facilitates high revisit times of the satellites therefore increasing possibility of obtaining cloud-free images. Previous research on image quality showed the Geoeye image

having better visual and radiometric quality than the WorldView image (Aguilar *et al.,* 2013).

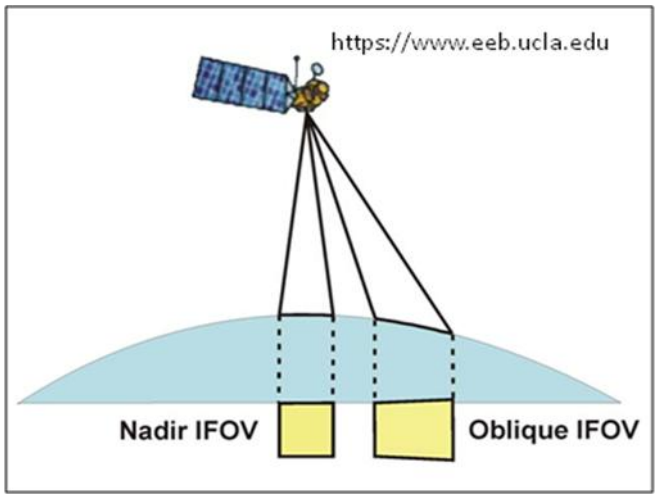

Figure 5: Nadir and oblique instantaneous fields of view of a satellite

Another major difference between the sensors is the number of spectral bands. Besides the four primary imaging bands, other bands such as Red Edge have been reported to offer more capabilities in feature recognition and discrimination as they allow the capture of finer spectral characteristics of a target. A study comparing WorldView 2 and IKONOS sensors showed improved results in the WorldView image, attributed not only to its spatial resolution but also the four additional bands (Pu & Landry, 2012). It is however important to note that during image acquisition, other factors beyond satellite characteristics such as atmospheric conditions, topography and sun angle during image acquisition play a considerable role in influencing usability of the resulting image (Aguilar *et al.,* 2013).

1.2 Sub-pixel classification methods

Commonly used land use and land cover classification techniques are pixel-based. However, the full potential of these conventional methods, otherwise referred to as hard classifiers, is limited by the presence of

mixed pixels (Figure 6). The phenomenon occurs when the spatial scale of a target is smaller than the resolution of the sensor (Foody, 2000; Kasetkasem *et al*., 2005).

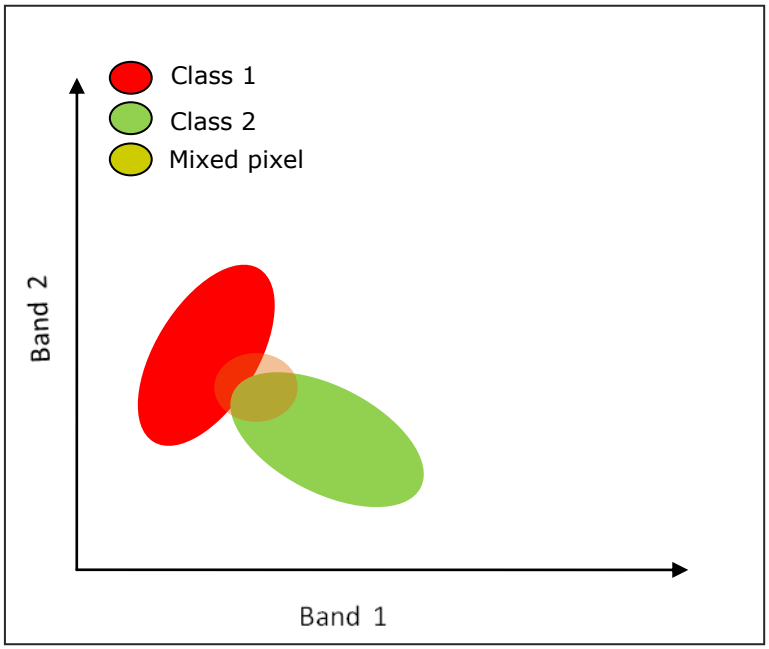

Figure 6: Representation of mixed pixel in a scatter plot

These pixels have been recognised as a major impediment to effective adoption of remotely sensed data. In reality, the assumption of full membership of a single class in a pixel does not always happen as pixels do not always represent areas of homogenous coverage of one class (Campbell, 1996). The adoption of subpixel classification methods attempts to resolve the mixed pixel problem.

In these approaches, the strength of membership a pixel displays to a class is used as a surrogate for fractional coverage of that class (Foody, 2000). The methods therefore allow soft proportions of each pixel to be partitioned between classes. The final output is in form of proportion images, each showing the relative abundance of each class within a pixel

(Tatem *et al*., 2002). These methods reportedly offer a more appropriate representation and accurate area estimations of land cover than their per-pixel counterparts (Lu & Weng, 2007). Techniques used in subpixel classification include Linear Spectral Unmixing (LSU), Nearest Neighbour classifiers and Multilayer Perceptrons (Tatem *et al*., 2002). Detailed description of some of the sub-pixel techniques can be found in Chapter 2.

1.3 Problem statement

Accurate mapping of mistletoe infestation is a serious concern. Current classification of remotely sensed imagery has not yet resulted in sufficiently accurate maps of mistletoe distribution. Attempts using pixel-based approach in the study area (Thapa, 2013) mapped mistletoe infestation based on the condition of Scots pine trees using Normalised Differential Vegetation Index rather than mistletoes. Low mistletoe detectability is attributed to the spatial scale in which it occurs, which is smaller than the resolution of current satellite imagery, therefore in this study, sub-pixel classification methods were proposed as a potential solution.

1.4 Research Objectives

General Objective

To assess the potential of sub-pixel classification methods in detecting and mapping Pine Mistletoe infestation

Specific objectives

1. To compare accuracies of Fuzzy Maximum Likelihood, Linear Spectral Unmixing, Super Resolution Mapping and Expectation Maximisation in mapping Pine Mistletoe infestation on Scots Pine trees

2. To investigate whether GeoEye 1 or WorldView 2 offers better detection of mistletoe infestation for specified classification techniques

1.5 Research Questions and Hypotheses

1. What is the distribution of mistletoe infestation in Bois Noir forest in Barcelonnette, France?

2. What is the most accurate subpixel classifier in mistletoe detection between Fuzzy maximum Likelihood, Linear Spectral Unmixing, Super Resolution Mapping and Expectation Maximisation?

   Ho: There is no significant difference in classification accuracy between the subpixel methods

3. How does accuracy of mistletoe infestation in GeoEye imagery compare with that of WorldView imagery for all methods

   Ho: There is no significant difference in accuracy of mistletoe detection between GeoEye 1 and WorldView 2 imagery

Chapter 2: Materials and Methods

2.1 Study area

Bois Noir forest is located in Barcelonnette basin, South Eastern France at Latitude 44º25'N and Longitude 6º40'E. It covers an area of 1.3 km^2 on the north-facing slope of the basin whose altitude ranges from 1,100 to 3000 metres above sea level (Maquaire *et al*., 2003). The Scots Pine forest, which is the subject of this project, is found in the upper half of the Bois noir forest and covers an area of about 0.6 km^2 between altitudes 1402 m and 1700 m. Figure 7 shows the location and land cover map of the study area.

Climate

Barcelonnette experiences strong inter-annual rainfall variability influenced by dry and mountainous Mediterranean intra-alpine zone. Annual rainfall is between 400 to 1100mm while the mean annual temperature is 7.5ºC (Flageollet *et al*., 1999). Rainfall in the basin varies in space, time and form: the lower parts of the basin receive more rainfall than snow during winter while for the upper part, precipitation is in the form of snow (Maquaire *et al*., 2003). Summer storms have been known to give rise to Hortonian runoffs with a strong erosive capacity after long dry periods.

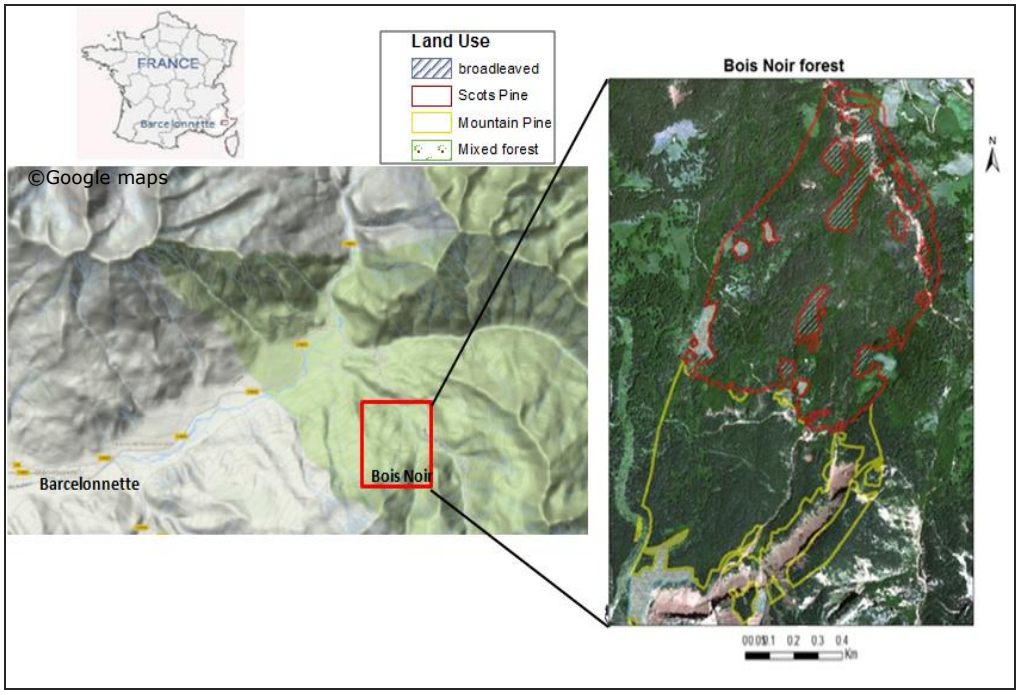

Figure 7: Location of the study area and land cover map overlain with the GeoEye image

Topography

The South-eastern French Alps are made up of sedimentary rocks which comprise alternating marl and limestone sequences dating back from Lias to Cretaceous period (Maquaire *et al*., 2003). The Barcelonnette basin has been subject to numerous landslides since 1850, with historical records revealing about 132 landslides by the year 2004. Several factors predispose the basin to geomorphological risks, among them lithology, tectonics and climate (Flageollet *et al*., 1999). Bois Noir forest is characterized by irregular topography with a slope gradient ranging from 10º to 70º. The soils are generally thin and poor which have an effect on tree formation. It is common to see drunken trees in Bois Noir forest due to the nature of soils and previous landslides.

Vegetation

The study area consists of 92% forest with monostands of conifers *i.e* Scots Pine *Pinus sylvestris* and Mountain Pine *Pinus uncinata* dominating the forest. Other coniferous stands include Norway spruce *Picea abies* and the European Larch *Larix decidua* (Mill.). Broadleaved tree species take up the least area and include Beech *Fagus sylvestris*, Ash *Fraxinus sp.* and Alder *Alnus sp*. The Scots pine forest is notably the only forest in the study area that has been infested by mistletoe and is the main subject of this study. The forest is largely a conservation area although occasional thinning of the trees has been done.

2.2 Materials and methods

2.2.1 Imagery

In this study, two satellite images were used: GeoEye 1 image acquired in June 2012 and WorldView 2 image obtained in September 2010. The GeoEye image was considered in this study because of a high spatial resolution of 2 m; and a near nadir field of view which has been reported to provide more accurate mapping (Ekstrand, 1996). In addition, the ability of the image to locate an object within just three meters of its physical location (Satellite Imaging Group, 2013) makes it appropriate for forestry studies. WorldView image, on the other hand, was selected because it contains eight imaging bands, an advantage during feature discrimination and classification. The four additional bands lacking in the GeoEye image are used for vegetation identification, analysis of vegetation condition and biomass studies. The image was collected from an off-nadir (oblique) field of view which, together with sun angle and terrain effects resulted in significant presence of shade. An aerial orthophoto (15 cm spatial resolution) covering the extent of the study area was used for georectification of the satellite images as well as for collecting training samples for classification. It was acquired in July 2009. Detailed

descriptions of the data sets, software and equipment used are provided in Annexes 1 and 2.

2.2.2 Description of sub-pixel methods

Fuzzy Maximum Likelihood

Fuzzy Maximum Likelihood (FML) (Wang, 1990) is a supervised classification method that softens outputs of crisp Maximum Likelihood (ML) classifier. The method is simple and robust and has been reported to provide more useful land cover information than ML. FML considers not only the mean vector but also covariance of a class and assumes that image data have normal distribution. FML gives a likelihood (probability) of a pixel belonging to a class by assigning membership ranging from 0 (absence of the class) to 1 (class fully covers a pixel). The membership grades can be related to proportions of land cover categories within a pixel (Maselli *et al*., 1995).The output images correspond to the number of categories, each having different grades of membership for a particular category. Training areas can be homogenous or heterogenous, provided that for the later, mixed proportions are known.

Linear Spectral Unmixing

Linear Spectral Unmixing is one method in mixed pixel classification that has mostly gained attention in hyperspectral imagery. LSU assumes that the reflectance spectrum recorded within a pixel is a linear combination of spectra of all components (endmembers) within the pixel (Adams et al., 1995). The assumption is based on the fact that no multiple scattering has occurred between different land cover classes so that each photon reaching a sensor has interacted with only one land cover component (Settle & Drake, 1993). The method uses the mean of an endmember to separate the different land cover components in an image and relies heavily on accurate selection of endmembers. According to Li *et al*. (2005), the criteria used to select a good endmember include spectral

uniqueness, linear independency and spatial generality. The end-product of LSU is a set of fractional images, each representing each identified endmember showing area proportions of the endmember within every pixel. Figure 8 shows the partitioning of a pixel into different classes with the output represented as proportion maps. Though LSU was originally developed for use on hyperspectral data, the technique has also been extended to multispectral datasets. However, there is a mathematical limitation on the maximum number of endmembers that can be specified. Some studies suggest a limit on endmembers to be equal to the number of spectral bands of the sensor plus one (Pacheco & McNairn, 2010; Hostert *et al.*, 2003). Other studies put a maximum limit to less than or equal to the number of spectral bands available (Weng & Lu, 2008; Atkinson *et al.*, 1997). Generally, the limit in number of classes depends on whether unconstrained or constrained LSU (sum of proportions of all classes in a pixel equals to one) is used.

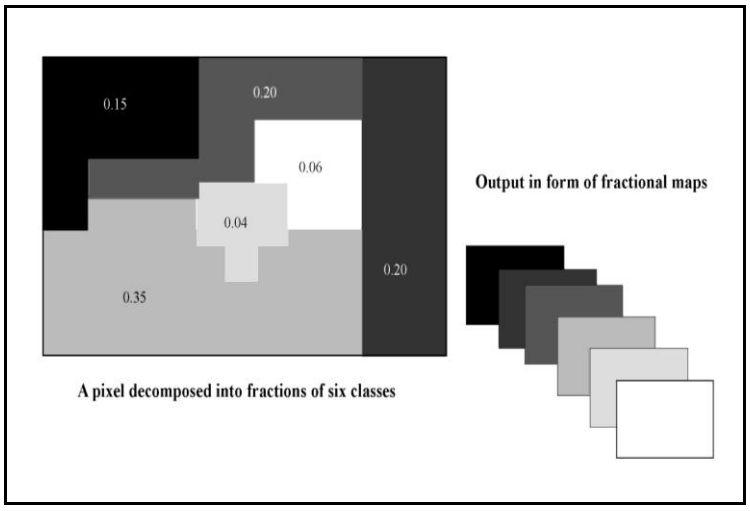

Figure 8: Class proportions and maps resulting from LSU method

Markov Random Field based Super Resolution Mapping

Previous studies on sub-pixel classification agree that land cover information obtained from the sub-pixel methods such as the mentioned LSU is useful and informative (Kasetkasem *et al*., 2005, Liu & Wu, 2005). However, these methods are limited by their inability to account for spatial distribution of the class proportions within a pixel (Atkinson *et al*., 1997; Verhoeye & Wulf, 2002). Super Resolution mapping (SRM) is therefore an alternative approach that considers spatial arrangement of classes between and within pixels. SRM works by decomposing a coarse pixel into sub-pixels and assigning class proportions to each subpixel. This technique ultimately increases the spatial resolution of the source image. Figure 9 shows degradation of a coarse resolution image to finer resolution in Super Resolution Mapping. Different statistical frameworks use SRM as a classification tool, among them Markov Random Field (Tolpekin & Stein, 2009).

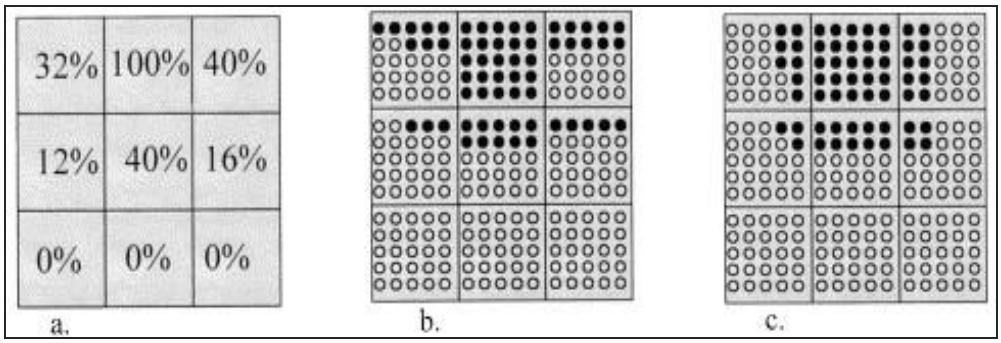

Figure 9: Illustration of Super Resolution Mapping of a 3x3 image (Atkinson, 1997). Image c. shows proportions and spatial distribution of one class in each pixel of the input image a.

Markov Random Field (MRF) theory is a branch of Bayesian probability theory that analyses spatial or contextual dependencies of physical entities (Tso & Mather, 2001). The approach is based on an optimization algorithm where raw coarse resolution images are first used to generate an initial sub-pixel classification. The initial stage uses Maximum Likelihood derived

probabilities to generate fraction images which are further processed to produce an initial super- resolution map (SRM) at fine spatial resolution (Kasetkasem *et al*., 2005). The initial SRM, together with the original coarse spatial resolution image and its estimated parameters are inputs to an iteration which refines the images by accurately characterizing the spatial dependence between the class proportions of the neighbouring pixels (Kasetkasem *et al*., 2005). Parameter setting is an important aspect when applying MRF. A good choice of parameters improves the classification result while a poor selection produces poor results (Tolpekin & Stein, 2009). Parameters include scale factor, a smoothness parameter (lambda), class mean and covariance. An output of SRM is a fine-scaled 'hard' classified image incorporating spatial distribution of classes within each coarse pixel.

Under MRF, pixels are not treated in isolation but are assumed to have a relationship with their neighbours. This however may be a drawback because while it assigns higher weights to homogenous regions than to the isolated pixels, loss of some small targets of interest may result (Kasetkasem *et al*., 2005). This is especially true for the mistletoe whose spatial scale is much smaller than its surrounding land cover components.

Expectation Maximisation

Expectation Maximisation (Dempster *et al.,* 1977) is a sub-pixel classification method that computes maximum likelihood estimates of a class given incomplete (limited) samples. The method involves two steps: Expectation (E) and Maximization (M). First, parameters for each cluster (the mean, covariance and the mixing coefficient) are randomly initialized. Then, given observed and unobserved data, the E-step computes the expected likelihood function of each data point belonging to each cluster. The step assigns pixels to clusters in a soft probabilistic way. Then the M-step finds the model parameters that maximize the likelihood (of the

cluster) obtained in E-step. The E and M steps keep alternating during iteration until convergence is reached (Weinstein, 2006).

EM is a generic algorithm and therefore needs to be adapted to a particular application. One of its primary applications is Gaussian Mixture modelling. EM models probability density function of a class by incorporating both covariance of class and the mean vector. The method uses a likelihood model for mixed pixels similar to that of SRM. However, unlike SRM which models a mixed pixel value using a single, normally distributed class, EM makes use of multimodal distribution of a class *i.e* a mixture of Gaussians (Figure 10).

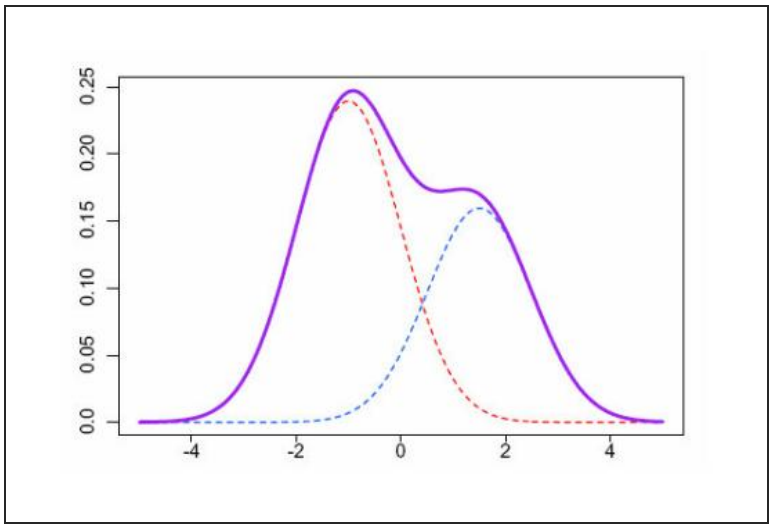

Figure 10: Multimodal distribution of a class modeled as separate classes

Flowchart

The overall flowchart showing the steps and methods used in this study is presented in Figure 11. It is divided into three stages: (1) field work, (2) image pre-processing, and (3) classification and accuracy assessment.

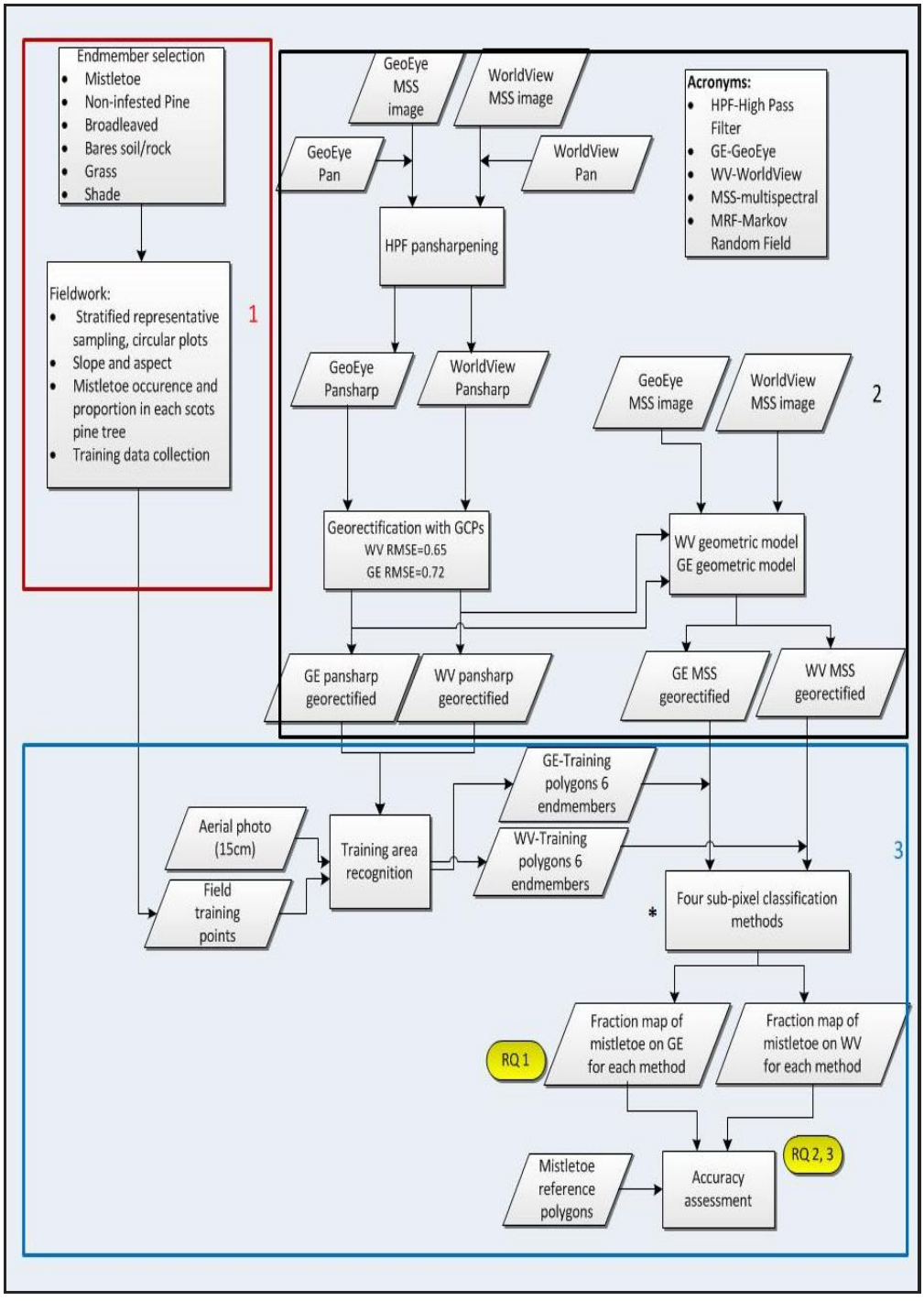

Figure 11: Workflow of applied methods
***** For detailed flowchart, see Figure 14

2.3 Selection of endmembers

Sampling design was geared towards obtaining areas in the field representative of the end-members for sub pixel classification. Identification of end-members is an important step in sub-pixel classification and accurate selection of the endmembers is even more crucial. The GeoEye sensor consists of four spectral bands thus a maximum limit of five land cover classes could be specified in LSU. However, because of variation in land cover, a few more classes can be added and has been observed to have no major effect on the LSU algorithm (personal communication with Tolpekin). The WorldView image on the other hand, contains eight imaging bands therefore it was not as restricted in the number of classes as the GeoEye dataset.

Based on visual inspection of the two images and after analyzing field data of Thapa (2013), the following six endmembers were defined: (1) mistletoes, (2) non-infested Scots Pine trees, (3) bare soil, (4) grass/undergrowth, (5) broadleaved trees, and (6) shade. The identified end-members were assumed to possess spectral reflectance responses unique to that specific land cover class.

2.4 Field work

Fieldwork was carried out in September 2013. Time was a serious limitation and could not allow collection of many samples and the possibility of trying out different sampling methods. In the field, areas representing five of the abovementioned endmembers were identified. For obvious reasons, shade was sampled from the image and not in the field. Field data obtained in year 2012 by Thapa (2013) showed areas of Scots Pine forest with varying degrees of mistletoe infestation. These data were used as a guide to identify target areas of mistletoe infestation for sampling. About 13 plots having heavy to medium infestation were sampled to represent the mistletoe class. A total of eight plots were sampled for the non-infested Scots pine class, eight plots for bare soil

class, and four plots for grass (undergrowth). This translated to a total of 33 training points sampled.

Stratified representative sampling method was used to obtain training samples for different endmembers. Detailed sampling was conducted in the Scots pine forest as this was the main area of interest in this study. For every sampled point within the pine forest, circular plots with a radius of about 12.6 m (corresponding to 500m^2) were delimited. The radius varied from 12 m to 13.5 m because of slope correction. Circular plots were preferred relative to rectangular or square plots because of the ease of sampling. A plot size of 500 m^2 has been reported to be an adequate sampling unit in vegetation studies, and is a preferred size in temperate zone forests (Nelder & Butler, 2008). In all classes, areas having more or less pure samples were targeted while heterogeneous areas were avoided. However, it was impossible to obtain an area representative of the pure mistletoe class, as it always grows within the canopy of pine tree (see Figure 3). Infested areas within the Scots Pine forest were actively searched in the field- this method was preferred over simple random sampling as there was a possibility that areas selected randomly could lack mistletoes. For the other classes, plots were equally distributed within the study area where general areas for sampling were selected after inspection of the images. For each sampled plot, GPS coordinates were obtained from the centre point.

Besides obtaining training data for image classification, additional variables were sampled relating mistletoe infestation intensity with aspect. Within the abovementioned Scots Pine sampling plots, slope steepness was measured in percentage and aspect recorded. Sampling was done at individual tree level and later infestation intensity was averaged for the entire plot. Only trees with a Diameter at Breast Height (DBH) larger than 10 cm were selected. Scots pine trees falling within

each plot were marked and their total number recorded. The proportion of mistletoes within each tree was then estimated at intervals of 10%. This allowed for ranking at a later stage to three major infestation classes on a scale of 0-3 where (0) corresponded to no infestation, (1) low infestation (>0-20%), (2) medium infestation (>20-40%) and (3) heavy infestation (>40%).

2.5 Image pre-processing

Pan-sharpening of the 2 m multispectral (MSS) images with respective panchromatic (0.5 m) band of both WorldView and GeoEye imagery for the purpose of classification was not recommended. This is because a very high spatial resolution would interfere with pixel unmixing process. Nonetheless, the procedure was done only to improve identification and delineation of training samples that would later be transferred to the multispectral images. A High Pass Filter pan-sharpening algorithm was used which has the advantage of maintaining high geometric precision of an image albeit with low colour information.

Although both GeoEye 1 and WorldView 2 images were obtained from the supplier while already geo-rectified, the geometries of the images were poor. The two images could not even align with each other. In various locations on both images, there was a shift of about 70-100 metres from the 'true' position. The true positions represent landmarks within the study area whose geographic coordinates were known and which had a perfect fit with the aerial orthophoto. Ortho-rectification of the images using a Digital Elevation Model was attempted but was not successful as the extent of the images and that of the DEM were not overlapping. Therefore, the pan-sharpened images were geometrically corrected using Ground Control Points (GCPs), with the aerial orthophoto as the reference image. Areas selected as GCPs were clearly visible on both aerial photo and pan-sharpened images such as forest path intersections, artificial structures such as a house, among other features. This was a complex task as

getting adequate points in a forested area proved cumbersome. Nonetheless, about six GCPs were selected for the WorldView image and seven GCPs for the GeoEye dataset. Nearest Neighbor resampling method and first degree polynomial transformation were applied. A Root Mean Squared Error of 0.65 and 0.72 were achieved for WorldView 2 and GeoEye 1 image respectively. An RMSE of half a pixel is considered acceptable.

For both datasets, the geometric models used for geo-referencing the 0.5 m pan-sharpened images were applied to their respective 2 m resolution MSS image to ensure a proper fit between both images. The objective was to accurately identify features and to collect training points on the pan-sharpened images and then transfer the points to the MSS image, the primary data for classification. Feature recognition on the pan-sharpened (0.5m) images of WorldView and GeoEye datasets improved to a greater extent when compared to the original MSS image. Standard deviation stretch was then applied to further enhance discrimination of the different vegetation components.

2.6 Classification and accuracy assessment

Training area recognition

Training polygons for the six endmembers were delineated on both pan-sharpened WorldView and GeoEye datasets. This was done using a combination of an aerial orthophoto (15 cm resolution) and training data from the field. Training samples for all endmembers (except shade) were majorly delineated on the aerial photo and were then transferred to the satellite image to locate their corresponding positions. For the mistletoe endmember, it was still not possible to accurately recognize mistletoes within the tree crowns even after pan-sharpening. Furthermore, there was still a small shift of about one metre in the images, despite the images having undergone the abovementioned geo-rectification. So, both the pan-

sharpened image and the aerial photo were juxtaposed and mistletoe polygons that had been created from aerial photos were placed on the exact location on crowns on satellite image (Figure 12). For the other classes, collection of training samples was rather straightforward. Because of variability within the grass and bare soil classes, a second set comprising eight endmembers was formed by splitting each of the two classes into two sub- classes. The final mistletoe training polygons for both WorldView and GeoEye images were then superimposed with their respective 2 m multispectral images and the fit was as expected. Classification was the next step.

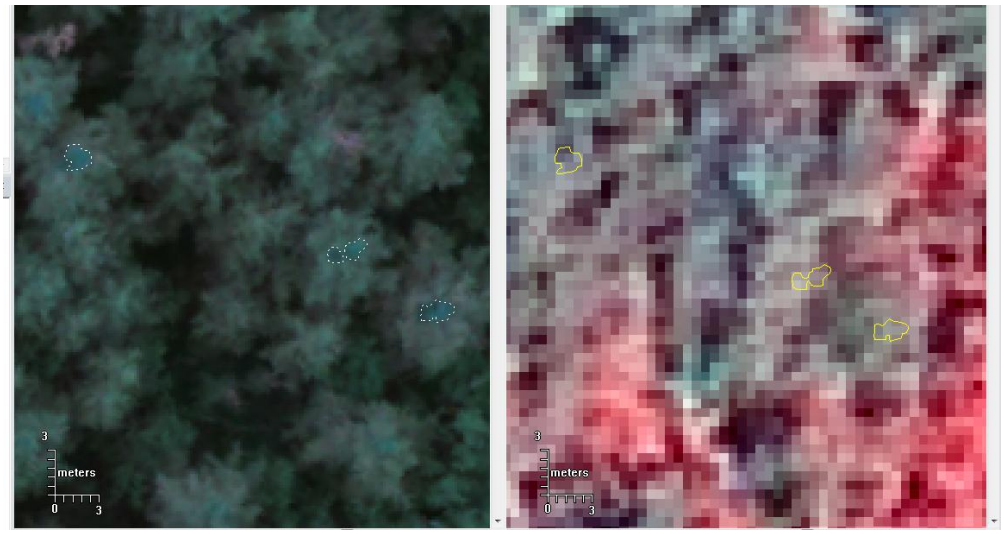

Figure 12: Mistletoe polygons on corresponding positions on (a) aerial photo and (b) pansharpened GeoEye image (RGB 4, 3, 2)

Image classification

A two-dimensional feature space was created for each image and for the two different-class models. Bands selected were those having high variation in spectral response between them as they provide more useful information. To obtain an accurate estimation of mistletoe proportion within a satellite pixel, the 15 cm aerial photo was classified using Maximum Likelihood method and draped over the satellite pixels. Mistletoe proportion could then be derived in the 2 m pixel (Figure 13). However,

there was a problem related to a shift between the aerial photo and satellite images. This made estimation of class area proportions difficult. The problem could be corrected by knowing the amount of shift for every pixel. Therefore, a code was developed in R (R Core Team, 2013) that spatial adjusted pixels in satellite images to align with the aerial photo. This was done only for the purpose of class proportion estimations on the aerial photo. In the diagram, the red pixel footprint and the purple polygon represent original position in the GeoEye image while the blue pixel footprint and the blue polygon are the shifted positions of the satellite pixels. Notice the shifted areas are now aligning with the classified mistletoe (yellow polygon).

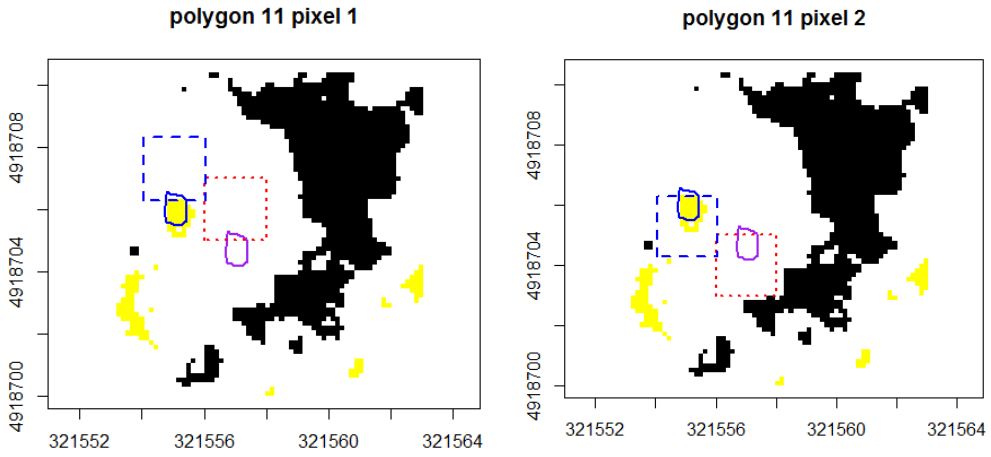

Figure 13: Mistletoe proportion within each overlapping GeoEye pixel footprint in the original and shifted positions. Yellow: mistletoes; black: shade; and white: uninfested pine trees

None of the mistletoe polygons fully occupied a satellite pixel. As a result, the mean and covariance could not be directly obtained with standard procedures. Two assumptions were made: (1) A linear mixture of two endmembers exists within mistletoe-infested areas: mistletoe and uninfested Scots pine trees. (2) Covariance of mistletoe class is estimated based on the ratio between spectral response of uninfested Scots pine and mistletoes on the aerial photo. Based on the two-class assumption, the

proportion of mistletoes as well as that of the Scots pine endmember were computed within each satellite pixel. Since the mean of the pine trees was known from its training set, the mean of the mistletoe endmember could be derived based on Linear Spectral Unmixing equation as follows:

$$R_b = \sum_{i=1}^{M} f_i r_{ib} + E_b$$

where R_b is pixel reflectance at band b, f_i is the fractional abundance of endmember i, M is the total number of endmembers, r_{ib} is the reflectance at band b of endmember i, and E_b is the residual error in band b of the model. Constrained LSU was used to limit the sum of proportions within a pixel to one.

Covariance of pine class on the satellite images was known. However, as indicated earlier, covariance for mistletoe class could not be directly obtained. The covariance matrix of both classes was available on the aerial orthophoto. The spectral ratio in the three bands (red, green, and blue) between pine trees and mistletoe was 4:1.The same relationship was assumed to exist on the satellite images, and therefore covariance of mistletoe class on the images was estimated.

Transformed Divergence

Transformed Divergence (TD), a commonly used class separability factor, was computed from the training set. TD is a measure of similarity between spectral signatures of classes, and takes values between 0 and 2, with no unit of measurement. Low TD values correspond to high confusion between classes and vice versa. Low class separability may affect classification accuracy (Richards & Jia, 2006). The formula for computing TD is:

$$TD_{ij} = 2(1 - e(-D_{ij}/8))$$

where *D* is Divergence. *D* is calculated based on mean and covariance of each class. It ranges from 0 to infinity; *i* and *j* are two classes under comparison. A contingency table (error matrix) was produced as well to ensure consistency in the training set. This was produced through a quick ML classification of training pixels. The matrix contains the number of pixels that are classified as expected.

Maximum Likelihood (ML) was initially applied. This procedure was done to assess whether classification results were realistic. Sub-pixel classification was thereafter done using the four methods described in the flowchart in Figure 14. Classification was tested for both six and eight classes to assess whether there would be any improvement in land cover discrimination.

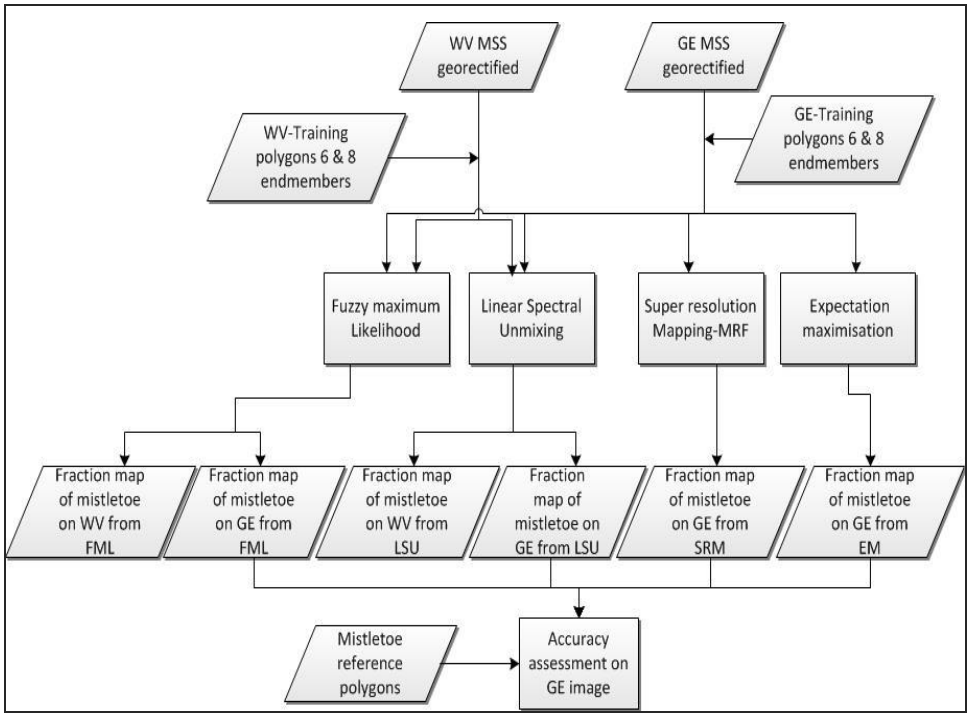

Figure 14: Detailed flowchart showing sub-pixel methods used in the order in which they appear

The first sub-pixel classifier to be applied was Fuzzy Maximum Likelihood classification. The classifier was selected because it is a simple and more robust method compared to Maximum Likelihood. However, visual interpretation and comparison of the results with the aerial orthophoto showed that mistletoe detection was unsatisfactory.

Considering that FML only gives a probability of mistletoe occurrence within a pixel, this may not have represented true endmember proportions. Linear Spectral Unmixing was therefore applied to map mistletoe occurrence in terms of fractional abundance. LSU was selected as it is a simple method just like FML and is among the most widely used sub-pixel classifiers. As explained before, the method uses class mean vector to classify an image of interest. However, LSU is limited by its

inability to consider variability within a class. This was confirmed by the resulting map, which did not represent true mistletoe infestation at all.

In light of the limitation of LSU, Markov Random Field based Super Resolution Mapping (SRM) and Expectation Maximisation methods were applied. These methods were preferred because they model probability density function of a class by incorporating both covariance and the mean vector. The two methods however differ in how they deal with distribution of data: SRM makes use of a single, normally distributed class whereas EM models class distribution as a mixture of Gaussians. Due to high processing demands by SRM, a subset of the GeoEye image was used. The subset and SRM parameters were put in an iterative process called Simulated Annealing till convergence was reached. Detailed description of Simulated Annealing can be found in Section 8.4.2 of Tso & Mather (2009). The super resolution property was not important; instead, SM was used for the purpose of obtaining subpixel proportions within pixels. Tolpekin and Stein (2009) observe that SRM can improve the initial class area proportion estimates. This is possible because of its probabilistic spectral mixture model. Expectation Maximisation method was applied at a scale broader than SRM and has the advantage of using relatively feasible computation time compared to SRM. EM was selected based on its ability to model incomplete observations, a problem faced in this study.

The outputs of the applied sub-pixel methods (except for SRM) were grayscale fractional images for each of the identified end-members. The image of interest to this study was the one representing the relative proportion of mistletoes per pixel. Each pixel represented mistletoe proportion on a scale ranging from 0 to 1. For SRM, the high spatially resolved map from SRM could be resampled to the original coarse resolution to obtain fractional map of mistletoe occurrence within the coarse resolution pixel. A final mistletoe infestation map was obtained from the fractional maps by grouping the proportion of mistletoes into

three main categories: >0-20% recorded as low occurrence; >20-40% as medium occurrence; and > 40% as high occurrence. This ranking was selected in this study because it was more practical based on observations of mistletoe infestation in the field.

Accuracy assessment

Root Mean Square Error (RMSE), Correlation Coefficient (*r*) and Coefficient of determination (R^2) were computed to evaluate the performance of FML, LSU, EM and SRM methods in mistletoe detection. However, this was based on training data because the mistletoe class had relatively fewer samples. It is worth noting that for SRM assessment, the smoothness parameter was set to zero (implying no prior information on spatial arrangement of classes). Simulated annealing was run using the most common starting parameters (starting temperature of 3 and updated at 0.99) to reach about 400 iterations. The procedure was repeated five times to ensure results were reproducible. Leave-One-Out Cross Validation (LOOCV) method was planned for all the applied methods to resolve the problem with limited number of mistletoe samples. The method was proposed if classification results were acceptable. Since none of the methods yielded tangible results, LOOCV approach was discarded. In this method, all samples except one are used for training, and the remaining one left for validation. The experiment is repeated for all samples such that eventually every sample is used for validation. This implies that for a dataset with N samples, N experiments are performed. The true error can then be estimated as the average error rate on validation samples. The drawbacks of this method are: it is computational demanding, and the resulting variance is high when different sets of samples are sampled from the same distribution (Elisseeff & Pontil, 2002).

Chapter 3: Results

3.1 Feature Space and Class Separability

Figures 15a and b show feature spaces of the six and eight endmembers identified between bands 3 (Red) and 4 (NIR) of the GeoEye image. Classes except for the mistletoe, grass and broadleaved trees were relatively distinct and could easily be discriminated in the feature space. The spectral signature of mistletoe pixels was completely enveloped by the uninfested class. However, the mistletoe cluster appearing in the feature space is an estimation of covariance of the mistletoe based on the covariance ratio between infested and uninfested pine trees on aerial photo (Section 2.6.2). Since there was no major difference in class separability between the eight- and the six-class sets (Table 1), classification results from the six-class model were presented.

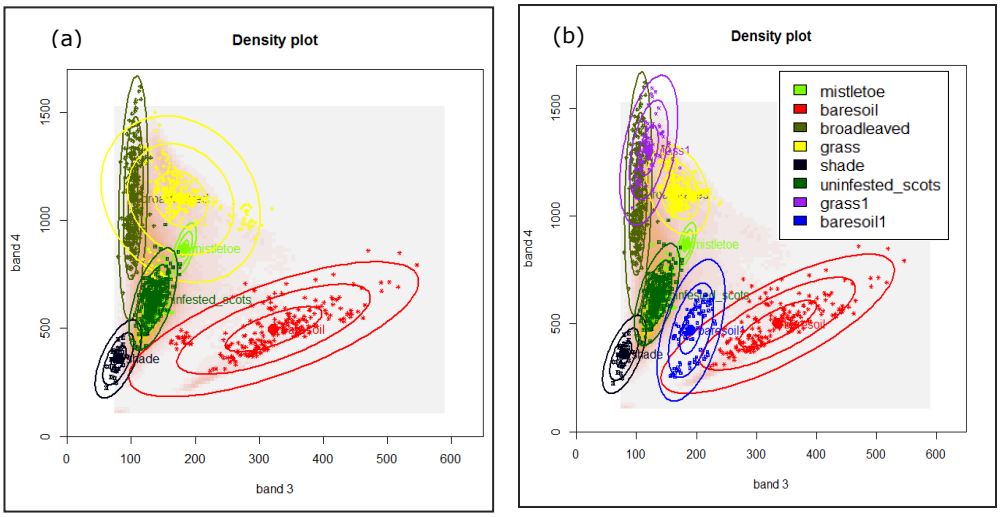

Figure 15: GeoEye density plots for (a) six classes (b) eight classes in Red and NIR bands. The three ellipses for each class represent three standard deviations of observations from the mean

Box plot results for green, red and NIR bands of GeoEye image showed the classes having variable ranges, as shown in Figure 16. Broadleaved class had the largest variance, the pine tree with moderate variance while mistletoe had the least. The box plot representing mistletoes could not be drawn as required because only the estimated mean and covariance were available. Plots for broadleaved and grass were at comparable heights yet different from mistletoes, implying more discrimination between the two classes from the mistletoe.

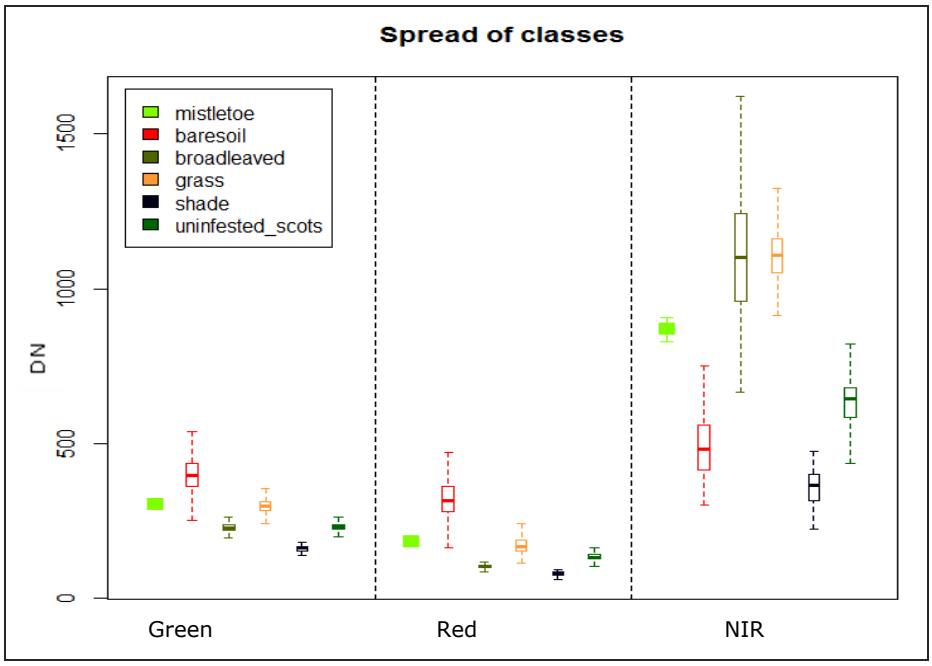

Figure 16: Box plot of endmembers within three bands of GeoEye image

For the WorldView 2 image, the endmember profiles were distinct between bands 5 (Red) and 7 (NIR), except for grass and uninfested pine classes (Figure 17). Similar to the GeoEye image, the mistletoe endmember was completely enveloped within the uninfested class while its estimated cluster was separate.

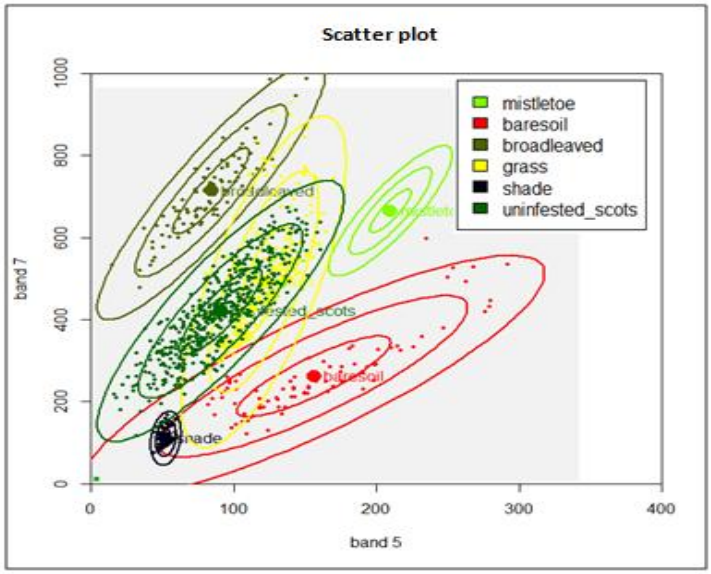

Figure 17: Feature space of endmembers between Band 5 (Red) and Band 7 (NIR) of WorldView 2 image**.** Three ellipses represent three standard deviations of data from the mean

Figure 18 shows the spread of the six endmembers in Green, Red and Near Infra Red bands of the WorldView 2 image. In the plots, within-class variance was consistently high for the bare soil and uninfested pine cases and lowest for shade class. The mistletoe cluster appears separated from uninfested pine in the shorter wavelength bands but overlaps with pine trees in the NIR bands.

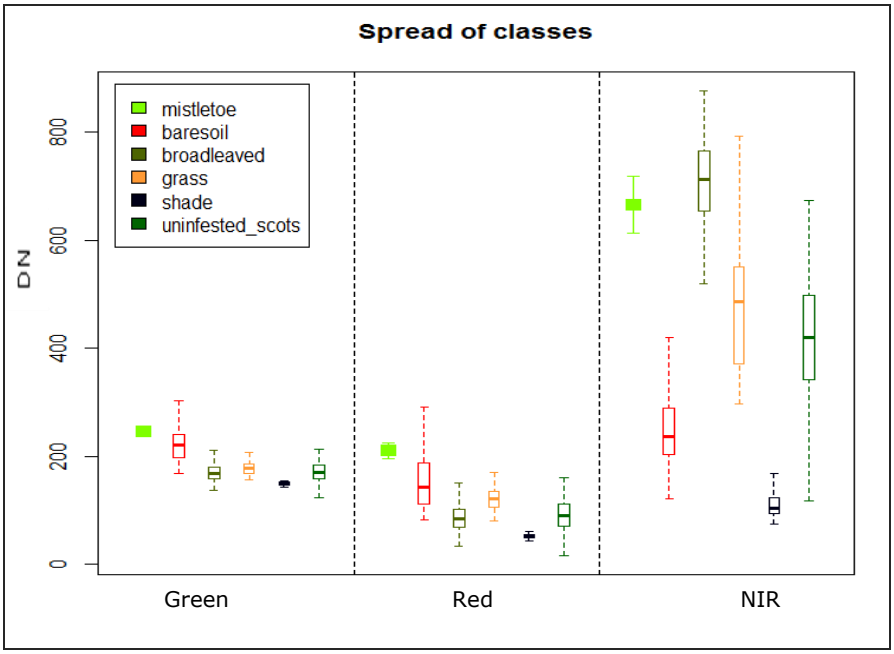

Figure 18: Boxplot of endmembers within three bands of WorldView image

Results of contingency analysis showed overall accuracy of 94.22 % for GeoEye image and 96.33% for WorldView image (Table 1). This test is not meant to provide an overall evaluation of classification but is done to ensure consistency in the training set. Results from both images show that except for mistletoe class, training set for the other classes were more or less consistent and well captured. None of the mistletoe pixels were detected as mistletoes, rather almost all were identified as *Scots*.

Table 1: Contingency table from training set classification for (a) GeoEye and (b) WorldView image

(a)	Mistl.	Baresoil	Broadl.	Grass	Shade	Scots
Mistl.	0	0	0	0	0	0
Baresoil	1	220	0	0	0	0
Broadl.	0	0	301	5	0	0
Grass	2	0	5	282	0	1
Shade	0	0	0	0	31	3
Scots	33	0	0	19	1	308
Overall accuracy 94.22%						

(b)	Mistl.	Baresoil	Broadl.	Grass	Shade	Scots
Mistl.	0	0	0	0	0	0
Baresoil	0	87	0	0	0	0
Broadl.	0	0	103	0	0	0
Grass	2	0	5	263	0	3
Shade	0	0	0	0	93	0
Scots	36	0	0	0	0	504
Overall accuracy 96.33%						

Analysis of the Transformed Divergence (TD) in the GeoEye and WorldView image showed good separability between mistletoe and other classes (Tables 2a, b and c). Although results show TD of 2 between mistletoes and other classes, interpretation of these results should be done with caution given that TD was computed using estimated covariance obtained from the ratio between the pine and mistletoe classes on aerial photo.

Table 2: Transformed Divergence for (a) GeoEye image with six classes, (b) with eight classes and (c) WorldView image

(a)	mistl	Baresoil	Broadl.	Grass	Shade	Scots
Mistl.	0	2	2	2	2	2
Baresoil		0	2	2	2	2
Broadl.			0	2	2	2
Grass				0	2	1.99
Shade					0	1.96
Scots						0

(c)	mistl	Baresoil	Broadl.	Grass	Shade	Scots
Mistl	0	2	2	2	2	2
Baresoil		0	2	2	2	2
Broadl.			0	2	2	2
Grass				0	2	1.99
Shade					0	2
Scots						0

(b)	mistl	Baresoil	Broadl.	Grass	Shade	Scots	Grass1	Soil1
Mistl.	0	2	2	2	2	2	2	2
Baresoil		0	2	2	2	2	2	2
Broadl.			0	2	2	2	1.43	2
Grass				0	2	2	1.82	2
Shade					0	1.96	2	2
Scots						0	2	2
Grass1							0	2
Soil1								0

3.2 Classification and accuracy assessment

3.2.1 Comparison of methods

Classification on GeoEye imagery using ML and three sub-pixel classifiers: fuzzy ML, LSU and EM are presented in Figure 19.

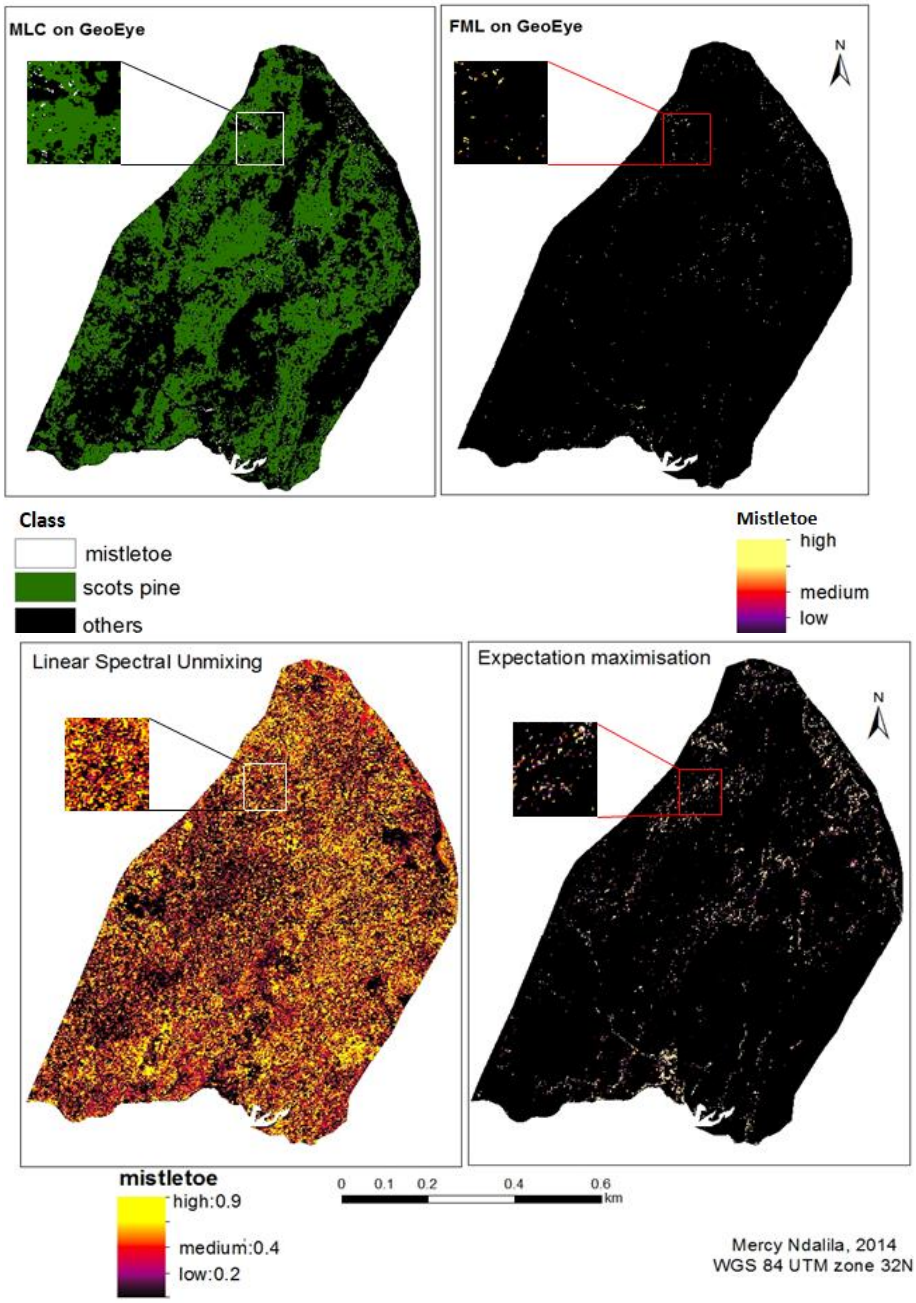

Figure 19: Mistletoe map from four methods on GeoEye image

MLC map has been included in Figure 19 for reference. Land cover classes not relevant to this study have been lumped as *others*. Mistletoe occurrence from the three subpixel methods is represented in terms of fractional abundance from low (<0.2), medium (0.2 to <0.4) to high (0.40 and above). Visual inspection of the maps revealed an inaccurate representation of mistletoe infestation. Detection using Fuzzy Maximum Likelihood method followed a similar trend as Maximum Likelihood and Expectation Maximisation methods. However, unlike EM, FML detected fewer areas with mistletoe infestation. On the other hand, Linear Spectral Unmixing consistently over-estimated mistletoe occurrence in most areas in the forest.

Despite a high Transformed Divergence between mistletoes and other classes, spectral confusion seemed to have occurred. All the tested methods suffered from a large degree of misclassification, where several areas classified as mistletoes were clearly belonging to grass, uninfested pine trees, broadleaved forest and surprisingly bare soil. SRM results have been provided separately in Figure 20 as they were based on a smaller subset. Parameters used during Simulated Annealing in SRM process include a smoothness parameter of 0.9 and scale factor of 3. The map has however not be separated into proportional maps for each class. Scots pine class has been included in the SRM map to allow easier interpretation and comparison with the aerial photo.

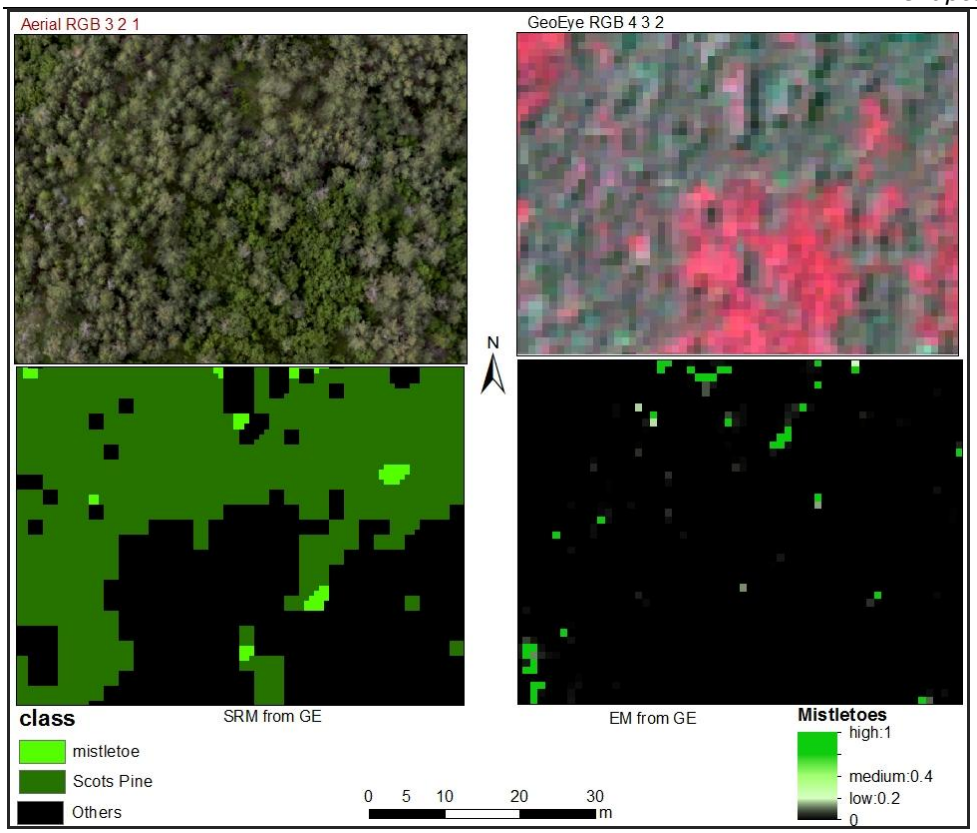

Figure 20: Results of SRM (below left), EM (below right), and subsets of aerial photo and 2m GeoEye image (above).Scots Pine class has been added to SRM map for ease of interpretation while the other four classes have been grouped as *others*

Just like the other sub-pixel methods, MRF-SRM did not produce an accurate representation of mistletoe infestation from visual inspection. Areas representing the pine class have been misclassified as mistletoes and the spatial extent of mistletoe occurrence is larger than in reality. A comparison between the classified images from SRM and EM methods (in Figure 20) shows some differences in mistletoe distribution, even though both methods use similar likelihood model for mixed pixels.

Overall, quantitative evaluation of the four sub-pixel classifiers (FML, LSU, SRM and EM) showed that accuracies were significantly low. Results of RMSE, correlation coefficient and coefficient of determination (R^2) with respect to mapping accuracies of the methods are presented in Figure 21

and Table 3. There was absolutely no agreement between observed mistletoe proportion and proportion predicted by all the methods (R^2 is almost zero). From the graphs, LSU and SRM under-estimated and overestimated mistletoe proportion whereas FML and EM consistently underestimated mistletoe occurrence.

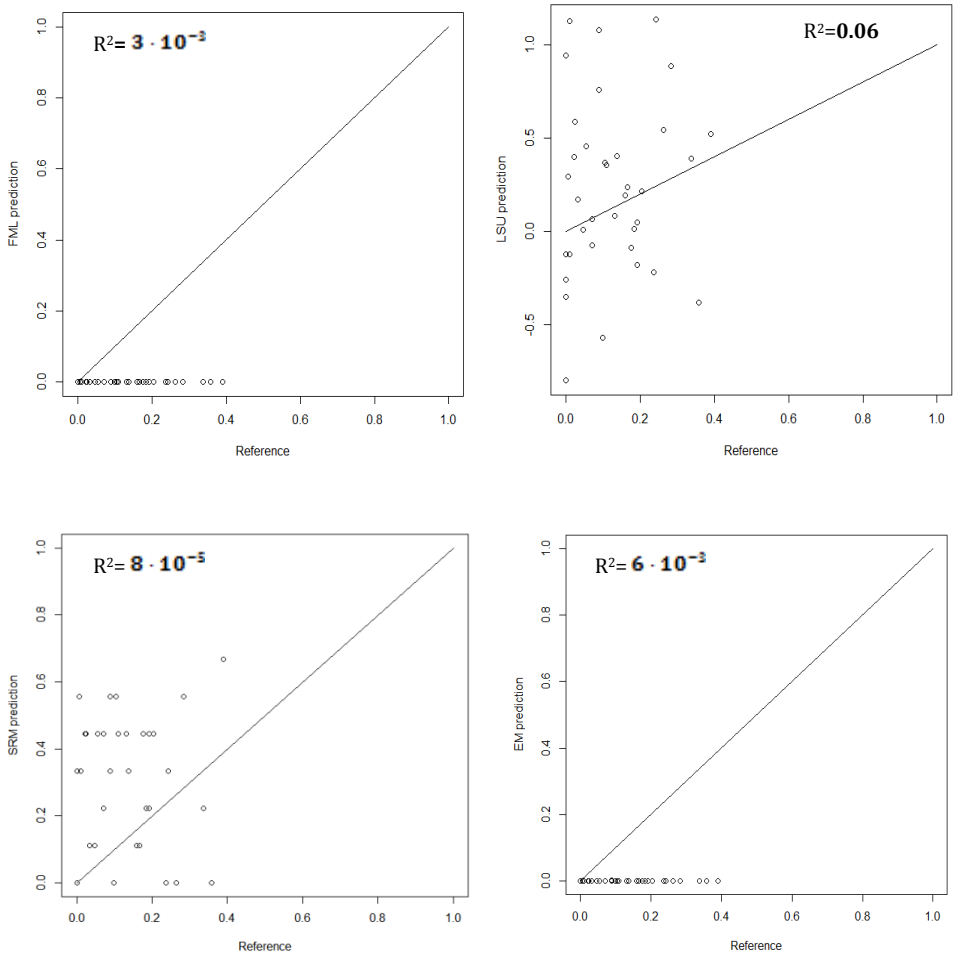

Figure 21: Correlation between predicted and observed mistletoe proportion in GeoEye image

Table 3: Agreement between observed and predicted mistletoe occurrence

Method	**RMSE**	**Correlation**	**R^2**
LSU	0.48	0.076	$6 \cdot 10^{-3}$
EM	0.166	-0.08	$6 \cdot 10^{-3}$
FML	0.166	-0.056	$3 \cdot 10^{-3}$
SRM	0.281	-0.009	$8 \cdot 10^{-5}$

Results of the tested methods were significantly poor such that the originally-planned leave-one-out cross tabulation would not be meaningful; it was therefore was abandoned. Similarly, due to poor performance, the methods could not be compared with previous Maximum Likelihood mapping of the same study area on WorldView 2 imagery.

3.2.2 Comparison of the datasets

Final infestation maps and accuracy assessment of the sub-pixel methods on the GeoEye image have already been described above. Accuracy assessment of the methods on the WorldView 2 image was not done largely because of imperfections appearing on the image. Therefore, comparisons of the two datasets were done visually. Visual inspection of LSU classification showed a poor classification on both images (Figure 22). Scan lines can be seen clearly on the map from the WorldView image.

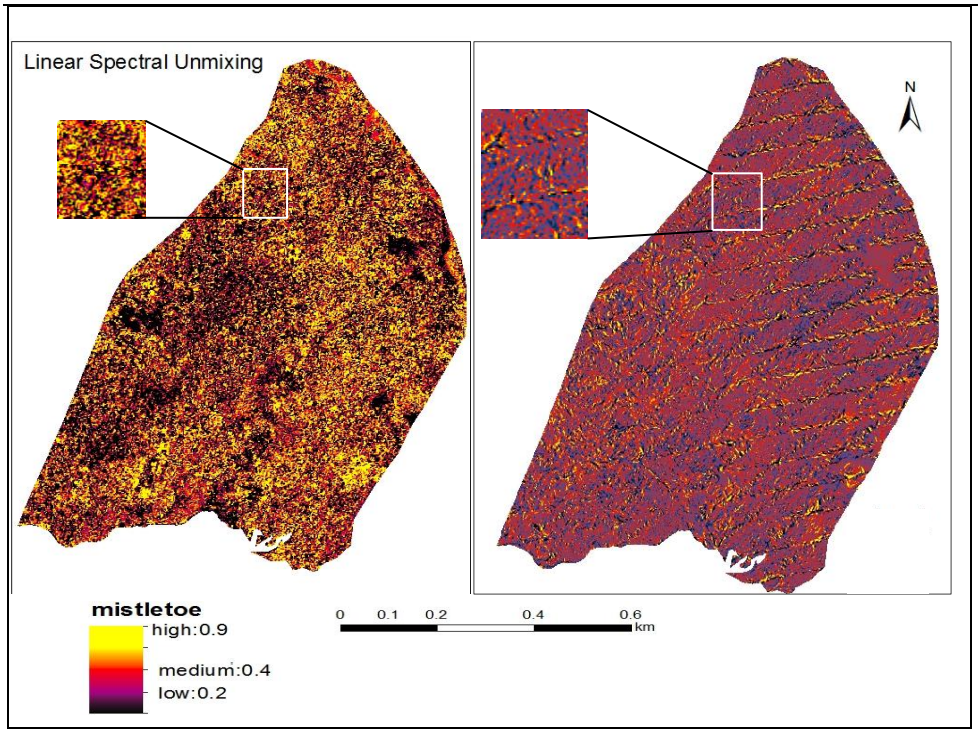

Figure 22: Comparison of LSU maps from (L) GeoEye and (R) WorldView image

The imperfections on the WorldView image were more pronounced in the LSU map than in the FML results (Figure 23). Just like the GeoEye image, LSU consistently overestimated mistletoe occurrence. Areas clearly belonging to the other classes were misclassified as mistletoes. For FML, the opposite was observed; mistletoe occurrence was under-represented. Due to significantly smaller mistletoe proportions, mistletoe occurrence on FML has been displayed in form of a point map. This is to facilitate visual interpretation.

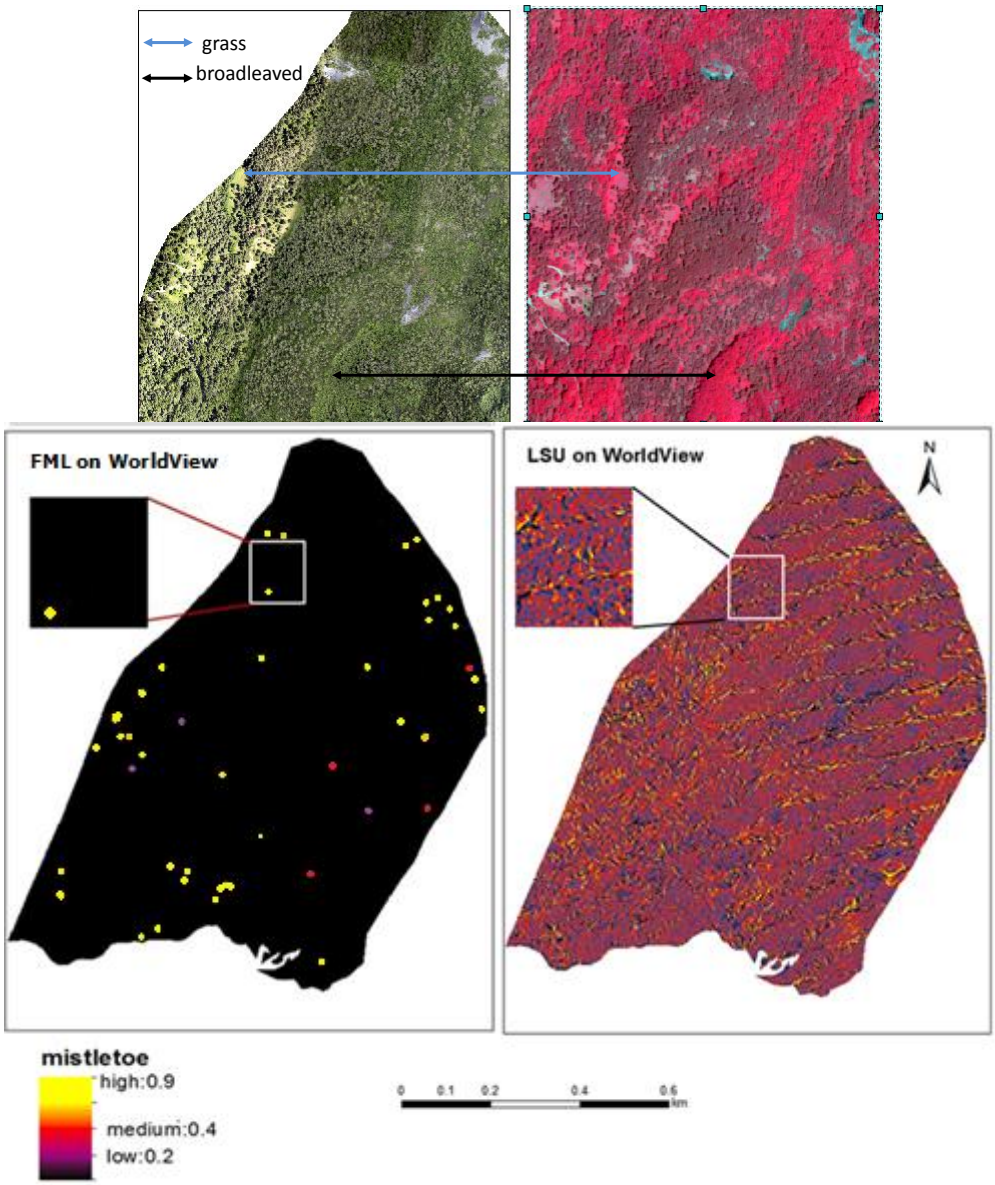

Figure 23: Infestation maps from FML and LSU methods on WorldView dataset. FML map contains mistletoe occurrence as points. Aerial photo and GeoEye image have been included for reference

These artifacts on the WorldView image impeded the analysis of influence of additional bands and the satellite viewing angle on accuracy of the

resulting maps. In fact, the results of both FML and LSU maps were not meaningful at all. Mapping using EM and SRM methods on WorldView image were not attempted as a result of poorly classified maps from the other mentioned methods.

Chapter 4: Discussion

4.1 Sub-pixel classification

From the findings, mapping accuracies of Linear Spectral Unmixing, Fuzzy Maximum Likelihood, Super Resolution Mapping and Expectation Maximisation were unexpectedly low. This study had hypothesised that sub-pixel methods would yield more accurate results because the mistletoe could be clearly distinguished within the crowns of the pine tree on the aerial orthophoto (Figure 12). However, application of the methods on the satellite images did not provide any reasonable detection.

From the results, none of the methods worked even though Transformed Divergence between mistletoes and other classes was maximum. Research shows that caution should be taken when interpreting results from class separability measures (Tso & Mather, 2009). The assumption of these approaches is that classes are normally distributed, and interclass variations are fully described by their covariance matrices. This does not always happen in reality and therefore using these separability measures may be misleading. Although previously reported pixel-based mapping in the same forest achieved an accuracy of 86% on WorldView 2 imagery, the results could not be compared with accuracies of the sub-pixel methods because it concerns the condition of Scots pine trees (NDVI) rather than the occurrence of mistletoe. A combination of factors that likely contributed to classification failure of the sub-pixel methods used in this study are discussed below.

Training samples

Training samples for mistletoe endmember were not representative. The size of the mistletoe relative to the pixel size of the images was small and hampered finding pure pixels for the mistletoe. A similar challenge was

also encountered in the field. Because of this spatial limitation, it was necessary that large number of mistletoe areas in the field and on the image be sampled. The idea was to collect as many observations with highest mistletoe infestation as possible. However, this was a challenge because (1) there was insufficient time in the field to obtain a large number of samples; (2) high within-class spectral variation of pine trees on the images did not allow accurate representation of mistletoe spectral profile. In addition, for most promising areas with mistletoes on the orthophoto, their corresponding locations on the images had a notable presence of shade. These frustrated efforts to obtain representative samples, resulting in a limited number of samples for mistletoe training. Various literature stress the importance of obtaining accurate training data (Heremans *et al*., 2011; Kavzoglu, 2009; Weng, 2008). Insuffcient data could reduce accuracy especially when variability within a class has not been captured. Collecting large number of samples ensures the variability within and between classes is correctly represented. This observation is consistent with findings by Weng (2008) who noted that insufficient and non-representative training samples often lead to poor classification results owing to inaccurate estimation of the mean vector and covariance matrix.

Determination of endmember statistics for mistletoes

Due to the smaller spatial extent of mistletoes within a pixel, the mean and covariance matrix for mistletoes could not be obtained directly. This was known beforehand, hence the idea was that during fieldwork, sufficient field observations of highly infested pine trees (with >40% mistletoes) were collected. This was to facilitate discrimination between mistletoe pixels and pure pine pixels. This however was not helpful as some of the field sampled mistletoe-infested areas were obscured by shade on the satellite images. Assumptions made to resolve the problem of no pure mistletoe class statistics could have contributed to lower

mapping accuracy. Firstly, the mean vector of the mistletoe obtained through LSU formula could have been inaccurately computed. Secondly, the estimation of mistletoe covariance based on ratio between spectral signatures of mistletoes and pine trees on the aerial photo may not have been correct. Consider too that the variability within the pine class on the images was considerably large, the estimation of mistletoe covariance could have been inaccurate. This explains enveloping of the mistletoe pixels in the uninfested pine class whereas the mistletoe cluster remained separate in the feature space (Figure 15).

Overall, the results demonstrate that class variance can significantly affect accuracy of a classification method when it is not considered. Heremans *et al*. (2011) observed that variability in class signatures had a major influence on the success of Artificial Neural Network classification.

Geometry of the images

Geometric distortions in the images were another probable source of classification error. These distortions were influenced by both topography and off-nadir field of view. While geo-rectification was necessary to improve the geometry and fit with other spatial data, there was a challenge of insufficient Ground Control Points. It is worth noting the importance of sufficient GCPs for accurate geometry fitting. However, obtaining enough GCPs in a natural forest can be a daunting task. Natural features are not preferred because of their irregular shapes and because the areas are prone to variations or changes (e.g. clearings). The inherent errors arising from geometrical correction could have contributed to reduced classification accuracy (Atkinson *et al*., 1997). These position errors affected estimation of mistletoe proportions from aerial photo for training. The shift between the images on the one hand and the photo on the other hand implied that the crowns on corresponding locations were not matching. Although a mechanical shift was applied to align both

datasets only for estimation purposes, errors could arise from this estimation.

Estimation of mistletoe proportions

Besides problems related to geometry, mistletoe estimation could also have lowered detection accuracy from the way mistletoe proportions were obtained. Training samples for mistletoes were acquired from aerial photos as opposed to the primary images. This approach was justified considering that mistletoes could not be detected visually on the satellite images. A problem however arises: aerial photos were first classified through Maximum Likelihood method and proportions of mistletoes and that of uninfested pine trees subsequently derived. The assumption therefore was that aerial photo classification was accurate (accuracy was not tested). This may not have been the case because not all areas where mistletoe was present in the classified image were correctly classified. To resolve this issue, mistletoe polygons (that aided estimation of mistletoes proportions) were only delineated in areas that were clearly infested on the aerial photos.

Sun angle and topography

Sun elevation angle during image acquisition has been found to affect results of land cover classification (Galvão *et al*., 2004, Ekstrand, 1996). The GeoEye and WorldView images used in this study were acquired at different times of the year, introducing sun illumination differences. The sun angle for WorldView image was 48 degrees while that of GeoEye image was 64 degrees. A low sun angle largely affected sun illumination resulting in considerable amount of shade in the WorldView image than in the GeoEye dataset. Although shade was considered as a separate endmember, the obscuring of spectral signal of pine trees could have

introduced classification errors in areas covered by shade. This is in reference to classification on the GeoEye image.

Topography is another factor that hinders extraction of information from multispectral imagery (Ju *et al*., 2008). Bois Noir forest is characterised by irregular terrain, with slope steepness ranging from 10-35º and in some sections up to 70º (see description of study area). The large slope gradient, in addition to the presence of tall trees in such areas cast shadows on areas beneath the slope. This could have caused misclassification of areas covered by shade. However, it should be noted that the magnitude of terrain effects was largely due to a low sun angle. This is evident in the GeoEye image, which had relatively fewer shadows even though the underlying terrain is the same for both datasets. Overall, a low sun angle and terrain effects caused shadows that hampered finding pixels for the non-infested and infested pine trees.

Image properties

The success of any method relies on the properties of input data (Kavzoglu, 2009). In this study, the image resolution of both satellite images may not have provided sufficient means of mistletoe mapping as desired. The 15 cm resolution of the aerial photo permitted better interpretation of mistletoe occurrence than the 2m resolution satellite images. Although very high spatial resolution imagery is desirable, new problems arise when such image data are used. Weng (2008) observed that high spatial resolution does not always lead to high classification accuracy due to the presence of shading as well as high spectral variation within a land cover class. Moreover, the associated costs could hinder adoption of very high resolution datasets such as aerial photography in forest infestation mapping (Wulder *et al.*, 2004).

A more specialised approach through the use of drones or Unmanned Aerial Vehicles (UAVs) could facilitate better mistletoe detection by overcoming the effects of costs in manned aircrafts as well as lower spatial resolution in satellites. UAVs have been widely used in military applications but have recently received attention in vegetation surveillance and monitoring, more so in forestry and precision agriculture (Berni *et al.,* 2009). UAVs are reliable alternatives when compared to piloted airborne systems and are better suited for local applications.

The WorldView image yielded completely different and incompatible results. The main difference with the GeoEye imagery stemmed from image quality. The presence of scan lines on WorldView image significantly hampered detailed analysis of the image. These imperfections came from errors in the sensor during image acquisition. Striping occurs when there is an imbalance in detectors. This results in radiometric errors, causing anomaly in spectral radiance (Carfantan & Idier, 2010). Although de-striping is a common procedure used to correct for the scan lines, the problem was detected late so the procedure was not attempted. Because of errors on the image, the influence of additional bands on mistletoe mapping did not seem to be important.

Although detection using the two satellite datasets was problematic in this study, other related studies demonstrate that detection and mapping with high spatial resolution satellite imagery is possible, with accuracies comparable to aerial photography. A case in point is detection of Mountain Pine damage by beetles in Northern America (White *et al.,* 2005). The authors used unsupervised clustering method to detect mountain pine beetle red attack on 4m IKONOS imagery. It should be noted that it is the condition of the tree that was mapped and not the actual cause. The

results indicated that accuracy of detection was 70.1% in low infestation stands, and 92.5% in areas with moderate infestation.

4.2 Aspect and mistletoe infestation

Initially the idea was to, apart from mapping mistletoe, assess the relation between mistletoe infestation and landscape properties (slope aspect) related to light climate (see Introduction). Aspect and mistletoe infestation intensities were therefore measured in the field. However, the observations were too few to warrant any robust statistical method and were therefore not included in the results section. Incidental observations in the entire landscape and previous work (Dobbertin *et al*., 2005; Hawksworth, 1959) confirm that aspect plays a role in the distribution and intensity of mistletoe infestation. Large slopes in the landscape that were exposed southwards (the other side of the valley on Figure 24) seemed to harbor abundant mistletoe bushes (personal observation). However, sampling about 25 plots within the study area revealed a different observation. There was no influence of slope direction on mistletoe distribution.

A possible explanation as to why field sampling did not reveal any significant influence is related to the general terrain in which the study area falls. Bois Noir forest is located in the larger north-exposed slopes (see placemark and north orientation symbol on Figure 24). Any local scale variations in slope direction that might have occurred seemed to have been insignificant in explaining mistletoe infestation.

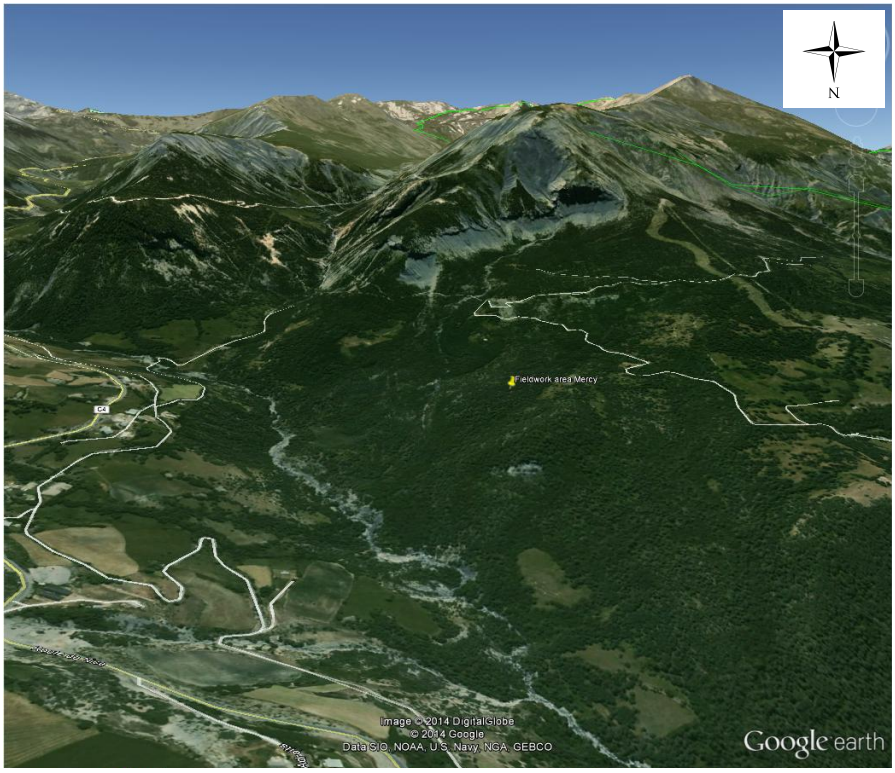

Figure 24: General terrain in which Bois Noir forest in located. Yellow placemark indicates the exact location of the forest

Literature confirms that mistletoe infestation tends to be more severe in areas exposed to sunlight (Zuber, 2004). North-exposed slopes are characterised by less sun illumination, lower surface temperature and high moisture level (Auslandera *et al.,* 2003). Consequently, mistletoe infestation is mostly not severe when compared with other slope expositions. Although this study considered aspect at a local scale, the findings suggest that future studies should consider slope exposition in relation to the scale of the landscape.

Chapter 5: Conclusion

This study was conducted to assess the potential of subpixel classification methods in mapping mistletoe infestation. Specifically, four sub-pixel classification methods (Fuzzy Maximum Likelihood, Linear Spectral Unmixing, Super Resolution Mapping and Expectation Maximisation) were tested to detect and map mistletoe infestation on very high resolution images within Bois Noir forest. These methods failed in detecting mistletoes within Scots pine forest, with almost no agreement between mapped and reference mistletoe proportions. A combination of several factors contributed to the mistletoe mapping classification failure. They ranged from non-representative training samples through to low sun angle in mountainous areas to geometric errors. Overall, a high spectral variability within classes, and especially the pine forest which is of importance to this study, introduced difficulties in separating mistletoes from the pine class. This can significantly affect accuracy of a classification method such as Linear Spectral Unmixing when it is not considered. Even for sub-pixel classifiers that incorporate variability within a class, class covariance may not have been adequately obtained.

Both WorldView and GeoEye imagery performed poorly for the applied sub-pixel methods. In addition to the observed low image quality of the WorldView dataset, both images did not seem to visually and quantitatively locate mistletoe-infested areas. The scale of mistletoe phenomenon did not permit accurate detection on the images despite the resolution of the images being the highest among currently operational satellites. As a consequence, the spectral signal generated by mistletoe is weak and consumed by the pine trees so that what is recorded is more representative of the pine trees.

Recommendations

The success of mapping relies not only on the classification method and the properties of the input data but also on the phenomenon under investigation. The following recommendations were proposed based on the results of this study:

- This study did not consider the influence of class variance on sub-pixel classification. Future research should be directed towards understanding the effect of within-class variability on performance of a classification method.
- More accurate mistletoe prediction would only be possible if remotely sensed datasets provide sufficient capabilities for detection. As they are currently, knowing the spatial limitation of mistletoes, detection with satellite imagery can be a challenging task. High resolution datasets such as Unmanned Aerial Vehicles could be investigated as a potential approach in overcoming the mentioned problems associated with low/inaccurate mistletoe detection and mapping. UAVs (also referred to as drones) may provide a more efficient means of detection to inform forest management decisions.
- To minimise the effects of low sun elevation angle, consideration should be made to utilise an image acquired at the time of the year when there is sufficient sun illumination. This reduces effects of shading on land cover materials.

References

Adams, J. B., Sabol, D. E., Kapos, V., Filho, R. A., Roberts, D. A., Smith, M. O. (1995). Classification of multispectral images based on fractions of endmembers: Application to land-cover change in the Brazilian Amazon. *Remote Sensing of Environment*, 52, 137−154

Aguilar, M. A., Saldaña, M. M., Aguilar, F. J. and Fernández I. (2013). Radiometric Comparison between GeoEye-1 and WorldView-2 Panchromatic and Multispectral Imagery

Atkinson, P., Cutler, M., Lewis, H. (1997). Mapping sub-pixel proportional land cover with AVHRR imagery. *International Journal of Remote Sensing,* 18, 917–935

Auslandera, M., Nevob, E. and Inbara, M. (2003). The effects of slope orientation on plant growth, developmental instability and susceptibility to herbivores. *Journal of Arid Environments* 55, 405–416

Barnsley, M.J. (1984). Effects of off-nadir viw angles on the detected spectral response of vegetation canopies. *International Journal of Remote Sensing*, 5(4), 715-728. doi:10.1080/01431168408948853

Berni, J., Zarco-Tejada, P.J., Suarez, L. and Fererez, E. (2009). Thermal and narrow band multispectral remote sensing fro vegetation monitoring from an unmanned aerial vehicle. *IEEE Trans. Geoscience and Remote Sensing*, 47(3), 722-738

Campbell, J.B. (1996). In Introduction to Remote Sensing, 2nd ed. Taylor & Francis, London.pp 62

Carfantan, H. and Idier, J. (2010). Statistical Linear Destriping of Satellite-Based Pushbroom-Type Images. *IEEE Transactions on Geoscience and Remote Sensing*, 48, 4

Chauvin, C. and Vallauri, D. (2002). Indicators for ecological restoration of degraded marl in the Southern Alps, 120 years after reforestation. *Journal of Ecology and Earth life,* vol. Supp. 9, pp. 241-250

Dempster, A., Laird, N. and Rubin, D. (1977). Maximum likelihood from incomplete data via EM algorithm. *Journal of the Royal Statistical Society, Series B*, 39(1), 1-38

Dobbertin, M., Hilker, N., Rebetez, M., Zimmermann, N. E.,Wohlgemuth, T., and Rigling, A. (2005). The upward shift in altitude of pine

mistletoe (*Viscumalbum* ssp. *austriacum*) in Switzerland - The result of climate warming? *International Journal of Biometeorology, 50*(1), 40-47.

Dobbertin, M., Rigling, A. (2006). Pine mistletoe (Viscum album ssp. austriacum) contributes to Scots pine (*Pinus sylvestris*) mortality in the Rhone valley of Switzerland. *Forest Pathology,* 36, 309–322

Ekstrand, S. (1996). Landsat TM forest damage assessment: correction for topographic effects. *Photogrammetric Engineering & Remote Sensing*, 62(2), 151-161

Elisseeff A. and Pontil M. (2002). Leave-one-out error and stability of learning algorithms with applications. Accessed on 04-01-2014. http://www0.cs.ucl.ac.uk/staff/m.pontil/reading/natoasi.pdf

Erdős, L., Méri, A., Bátori, Z., Gallé R. and Körmöczi, L. (2012). North-south facing vegetation gradients in the villainy mountains: A case study on the population and the community level. *Pak. J. Bot.,* 44(3), 927-932.

Fischer, J.T. (1983). Water relations of mistletoes and their hosts. In: Calder M, Bernhard T (eds) The biology of mistletoes. Academic Press, Sydney, pp 163–184

Flageollet, J.C., Maquaire, O., Martin, B., and Weber, D. (1999). Landslides and climatic conditions in the Barcelonnette and Vars basins (Southern French Alps, France). *Geomorphology, 30*(1–2), 65-78. doi: http://dx.doi.org/10.1016/S0169-555X(99)00045-8

Foody, G. M. (2000). Estimation of sub-pixel land cover composition in the presence of untrained classes. *Computers & Geosciences, 26*(4), 469-478. doi: http://dx.doi.org/10.1016/S0098-3004(99)00125-9

Galvão, L. S., Ponzoni , F. J. Epiphanio , J. C. N., Rudorff , B. F.T. and Formaggio, A. R. (2004). Sun and view angle effects on NDVI determination of landcover types in the Brazilian Amazon region with hyperspectral data. *International Journal of Remote Sensing*, 25:10, 1861-1879, DOI: 10.1080/01431160310001598908

Gottfried, G.J. and Embry, R.S. (1977). Distribution of Douglas Fir and Ponderosa pine dwarf mistletoes in virgin Arizona mixed conifer stand. Research paper RM-192. US Department of Agriculture

Hawksworth, F.G. (1959). Distribution of dwarf mistletoes in relation to topography on the Mescalero Apache Resrervation, New Mexico. *Journal of Forestry*, 57:919-022

Heremans, S., Bossyns, B., Eerens, H., and Van Orshoven, J. (2011). Efficient collection of training data for sub-pixel land cover classification using neural networks. *International Journal of Applied Earth Observation and Geoinformation, 13*(4), 657-667. doi: http://dx.doi.org/10.1016/j.jag.2011.03.008

Hostert, P., Röder, A., & Hill, J. (2003). Coupling spectral unmixing and trend analysis for monitoring of long-term vegetation dynamics in Mediterranean rangelands. *Remote Sensing of Environment, 87*(2–3),183-197. doi: http://dx.doi.org/10.1016/S0034-4257(03)00145-7

Ju, C., Cai, T. and Yang, X. (2008). Topography-based modeling to estimate percent vegetation cover in semi-arid Mu Us sandy land, China. *Computers and Electronics in Agriculture*, 64 (2), 133-139

Kavzoglu, T. (2009). Increasing the accuracy of neural network classification using refined training data. *Environ. Model. Softw.* 24, 850–858

Kasetkasem, T., Arora, M., Varshney, P.K. (2005). Super-resolution land cover mapping using a Markov random field based approach. *Remote Sensing of Environ*ment, 96, 302–314.

Kołodziejek, J., Patykowski, J., and Kołodziejek, R. (2013). Distribution, frequency and host patterns of European mistletoe (Viscum album subsp. album) in the major city of Lodz, Poland. *Biologia, 68*(1), 55-64. doi: 10.2478/s11756-012-0128-4

Liang, S. (2004). Quantitative Remote Sensing of Land Surfaces. John Wiley & Sons, Inc. New Jersey

Li, L., Ustin, S.L. and Lay, M. (2005). Application of multiple endmember spectral mixture analysis (MESMA) to AVIRIS imagery for coastal salt marsh mapping: a case study in China Camp, CA, USA. *International Journal of Remote Sensing*, 26, 5193–5207

Lu, D. and Weng, Q. (2007). A survey of image classification methods and techniques for improving classification performance. *International Journal of Remote Sensing,* 28 (5), 823–870

Maquaire, O., Malet, J. P., Remaître, A., Locat, J., Klotz, S., and Guillon, J. (2003). Instability conditions of marly hillslopes: towards landsliding or gullying? The case of the Barcelonnette Basin, South East France. *Engineering Geology, 70*(1–2), 109-130. doi: http://dx.doi.org/10.1016/S0013-7952(03)00086-3

Maselli, F., Conese, C., de Filippis, T. and Norcini, S. (1995). Estimation of Forest Parameters Through Fuzzy Classification of TM Data. *IEEE Transactions on Geoscience and Remote Sensing,* 33 (1)

McIntosh, R.L. (2004). Dwarf Mistletoe: Ecology and management. Forest Service, Saskatchewan Environment report

Merrill L.M., Hawksworth F.G. and Jacobi W.R. (1987). Frequency and severity of Ponderosa pine Dwarf Mistletoe in relation to habitat type and topography in Colorado. *Plant disease,* 71:342-344

Mistletoe Matters. (2012). Mistletoe Distribution in the UK. http://mistletoe.org.uk/homewp/wpcontent/uploads/2012/07/infosheet_1_Distribution.pdf. Accessed on 05-08-2014

Nelder, V.J and Butler, D.W. (2008). Is 500m^2 an effective plot size to sample floristic diversity for Queensland's vegetation? *Cunninghamia* 10(4): 513–519

Nierhaus-Wunderwald, D. & Lawrenz, P. (1997). ZurBiologie der Mistel. – *Merkblatt Praxis* 28, 1–8

Pacheco, A., and McNairn, H. (2010). Evaluating multispectral remote sensing and spectral unmixing analysis for crop residue mapping. *Remote Sensing of Environment, 114*(10), 2219-2228. doi: http://dx.doi.org/10.1016/j.rse.2010.04.024

Paine, T.D. and Baker, F.A. (1993). Abiotic and biotic predisposition. In: Schowalter, T.D., Filip, G.M. (Eds.) Beetle-Pathogen Interactions in Conifer Forests. Academic Press, pp. 61–79

Pu, R., Gong, P., Tian, Y., Miao, X., Carruthers, R., and Anderson, G. (2008). Invasive species change detection using artificial neural networks and CASI hyperspectral imagery. *Environmental Monitoring and Assessment, 140*(1-3), 15-32. doi: 10.1007/s10661-007-9843-7

Pu R. and Landry, S. (2012). A comparative analysis of high spatial resolution IKONOS and WorldView-2 imagery for mapping urban tree species. *Remote Sensing of Environment*, 124 ,516-533.

R Coe team. (2013). R: A language and environment for statistical computing. R Foundation for Statistical Computing, Vienna, Austria. URL http://www.R-project.org/

Razak, K. A., van Westen, C., Straatsma, M., Jean-Philippe Malet, J.P. and de Jong S. M. (2010). Airborne Laser Scanning as an effective tool for disaster mapping over mountainous forested landscapes. *Geophysical Research Abstracts*, 12 (7192)

Richards, J. A.and Jia, X. (2006). Remote Sensing Digital Image Analysis: An introducution, 4th ed. New York

Roura-Pascual, N., Brotons, L., Garcia, D., Zamora, R., and de Caceres, M. (2012). Local and landscape-scale biotic correlates of mistletoe distribution in Mediterraean pine forests. *Forest Systems, 21*(2), 179-188. doi: 10.5424/fs/2012212-02155

Satellite Imaging Corporation (2013). http://www.satimagingcorp.com/satellite-sensors/geoeye-1.html. Accessed on 12-08-2013

Sanguesa-Barreda, G., Linares, J. C., and Camarero, J. J. (2012). Mistletoe effects on Scots pine decline following drought events: Insights from within-tree spatial patterns, growth and carbohydrates. *Tree Physiology, 32*(5), 585-598. doi: 10.1093/treephys/tps031

Settle, J. and Drake, N. (1993). Linear mixing and the estimation of ground cover proportions. *International Journal of Remote Sensing*, 14, 1159–1177

Tatem, A. J., Hugh, G., Atkinson, P. M., and Nixon, M. S. (2002). Super-resolution land cover pattern prediction using a Hopfield Neural Network. *Remote Sensing of Environment*, 79, 1–14.

Thapa, S. (2013). Detection and mapping of incidence of *Viscum album* in pinus sylvestris forest of southern french alpe using satellite and airborne optical imagery. MSc. thesis, University of Twente, Enschede. Accessed 30-06-2013 http://www.itc.nl/library/papers_2013/msc/nrm/thapa.pdf

Tkacz, B., Moody, B., Castillo, J.V. and Fenn, M.E. (2008). Forest health conditions in North America. *Environmental Pollution*, 155: 409-425

Tolpekin, V. and Stein, A. (2009). Quantification of the effects of land-cover-class spectral separability on the accuracy of markov-random-field-based super resolution mapping. *IEEE Transactions on Geoscience and Remote Sensing*, 47, 3283–3297

Tso B. and Mather, P.M. (2001). Classification methods for remotely sensed data. Taylor & Francis, New York

Tso B. and Mather, P.M. (2009). Classification methods for remotely sensed data. 2nd ed, CRC Press, New York

Verhoeye, J. and Wulf, R. D. (2002). Land cover mapping at sub-pixel scales using linear optimization techniques. *Remote Sensing of Environment*, 79, 96–104

Wang, F. (1990). Fuzzy supervised classification of remote sensing images. *IEEE Transactions on Geoscience and Remote Sensing*, 28:194201

Watson, D.M. (2001). Mistletoe- A keystone resource in forests and woodlands worldwide. *Annu. Rev. Ecol. Syst*. 32:219-249

Weinstein, E. (2006). Expectation Maximisation Algorithm and applications. Courant Institute of Mathematical Sciences. Accessed on 05-04-2014 http://cs.nyu.edu/~eugenew/publications/em-talk.pdf

Weng, Q. and Lu, D. (2008). A sub-pixel analysis of urbanization effect on land surface temperature and its interplay with impervious surface and vegetation coverage in Indianapolis, United States. *International Journal of Applied Earth Observation and Geoinformation, 10*(1), 68-83. doi: http://dx.doi.org/10.1016/j.jag.2007.05.002

White JC, Wulder MA, Brooks D, Reich R and Wheate R. (2005). Mapping Mountain Pine Beetle infestation with high spatial resolution satellite imagery. *Remote Sensing of Environment*. 96:240–251.

Wierzbicki, G., Ostrowski, P., Mazgajski, M., and Bujakowski, F. (2013). Using VHR multispectral remote sensing and LIDAR data to determine the geomorphological effects of overbank flow on a floodplain (the Vistula River, Poland). *Geomorphology, 183*(0), 73-81. doi: http://dx.doi.org/10.1016/j.geomorph.2012.06.020

Wulder, M.A., Dymond, C.C. and Erickson, B. (2004). Detection and monitoring of the mountain pine beetle. Natural Resources Canada, Canadian Forest Service, Pacific Forestry Centre. Information Report BC-X-398. 28p.

Zuber, D. (2004). Biological flora of Central Europe: Viscum album L. *Flora - Morphology, Distribution, Functional Ecology of Plants, 199*(3), 181-203. doi: http://dx.doi.org/10.1078/0367-2530-00147

Annexes

Annex 1: Datasets used in the project (Satellite Imaging Corporation, 2013)

Characteristic	**GeoEye 1**	**WorldView 2**
Acquisition date	26th June 2012 during cloud-free and leaf-on conditions	13th September 2010 during cloud-free and leaf-on conditions
Image registration	Standard Geometic correction but with some geometric distortions	Standard Geometic correction but with notable geometric distortions
Spatial resolution	Panchromatic - 0.5m Multispectral- 2m	Panchromatic - 0.5m Multispectral- 2m
Number of bands ans spectral ranges	Four bands: Blue: 450 - 510 nm Green: 510 - 580 nm Red: 655 - 690 nm Near Infra Red: 780 - 920 nm	Eight bands: Coastal: 400-450nm Blue: 450-510nm Green: 510-580nm Yellow: 585-625nm Red: 630-690nm Red Edge: 705-745nm Near Infra Red 1: 770-895nm Near Infra Red 2: 860-940nm
Revisit time	< 3 days	1.1 days at nadir, 3.7 days at 20° off nadir
Swath width	16.4 km at nadir; 1,355km off nadir (45 °)	15.2km
Orbital altitude	770km	681km
Nodal crossing	10.30am	10.40am

Annex 2: Summary of equipment and software used during project implementation

	Equipment/software	**Description**	**Purpose**
1	GPS receiver	Equipment	Navigation and recording geographical coordinates
2	Clinometer	Equipment	Measuring slope
3	Compass	Equipment	Recording slope direction
4	Tape measure	Equipment	Delineating sampling plots
5	Camera and binoculars		Measuring crown cover and estimating mistletoe proportion in trees
6	ArcGIS 10.1	Software	GIS analysis
7	Erdas Imagine 2013 and ENVI 5	Software	Image analysis
8	R studio	Software	Image classification and Statistical analysis

Annex 3: R programming code used in this study

```
##Defining the root directory
Root <- "G:/Programming/Mercy"
Path_in <- paste(Root, "/Input",sep="")
Path_out <- paste(Root, "/Output",sep="")
dir.create(Path_out,showWarnings=FALSE, recursive=TRUE)
hist.stretch <- function(x)
## Read image ================================
image.fn <- "final_GG_image_9feb.img"
D <- readGDAL(paste(Path_in,"/",image.fn,sep=""))
Nb <- dim(D@data)[2]
#D.image <- D
#D.image@data <- hist.strecth(D@data)
proj_image <- D@proj4string
# Read vector data: training set=======================
fn.trset <- "final_gg_polygon_28feb1"
Pol <- readOGR(dsn=paste(Path_in,"/Subsets",sep=""), layer=fn.trset)
Ncl <- length(levels(Pol@data$class))
n.pol <- nrow(Pol)
# Compute class stats ====================
mu <- array(NA,c(Ncl,Nb))
Cov <- array(NA,c(Ncl,Nb,Nb))
Cinv <- array(NA,c(Ncl,Nb,Nb))
roi <- data.frame(array(NA,c(0,2)))
```

```
for(k in 2:Ncl)
{
        #pols <- which(as.numeric(unlist(Pol$Genus))==k)
        pols <- which(Pol$class_id==k)
        in.class <- array(0,nrow(xy))
        if(length(pols)>0)
        for(i in 1:length(pols))
        {
                j <- 1
                poly.xy <- coordinates(Pol@polygons[[pols[i]]]@Polygons[[j]])
                tmp <- point.in.polygon(xy[,1],xy[,2],poly.xy[,1],poly.xy[,2])
                ind <- which(tmp==1)
                in.class[ind] <-1
        }
        ind <- which(in.class==1)
        #length(ind)
                if(length(ind)>Ncl)
        {
                y <- D@data[ind,]
                roi <- rbind(roi,cbind(ind,rep(k,length(ind))))
                                mu[k,] <- colMeans(y)
                Cov[k,,] <- cov(y)
                Cinv[k,,] <- solve(Cov[k,,])
        }
}
## treat mistletoe class separately====================
tmp <- read.table(paste(Path_in,"/num_of_pixels_GG.txt",sep=""))
npix <- tmp[]
n.mist <- dim(npix)[1]
prop <- array(0,c(n.mist,4))
shade_prop <- array(0,c(n.mist,4))
pix_ids <- array(0,c(n.mist,4))
in.class <- array(0,nrow(xy))
tmp <- read.table(paste(Path_in,"/mistl_pixels_GG.txt",sep=""))
pix_ids[,] <- as.numeric(data.matrix(tmp[,]))
tmp <- read.table(paste(Path_in,"/mistl_prop_GG.txt",sep=""))
prop[,] <- as.numeric(data.matrix(tmp[,]))
tmp <- read.table(paste(Path_in,"/shade_prop_GG.txt",sep=""))
shade_prop[,] <- as.numeric(data.matrix(tmp[,]))
# Calculation mean of mistletoe class from Linear Unmixing========
Ntr <- sum(npix)
X <-array(NA,c(Ntr,3))
M <- array(0,c(3,Nb))
ind <- which(t(pix_ids)!=0)
ids <- as.vector(t(pix_ids))
ids <- ids[ind]
Y <- D@data[ids,]
X[,1] <- (as.vector(t(prop)))[ind]
X[,2] <- (as.vector(t(shade_prop)))[ind]
tmp <- X[,1]+X[,2]
X[,3] <- -tmp + 1
```

```
M[2,] <- mu[5,]
M[3,] <- mu[6,]
G <- array(0,dim(Y))
for(i in 1:Ntr)
for(k in 1:Nb)
{
  G[i,k] <- Y[i,k] - (X[i,2]*M[2,k] + X[i,3]*M[3,k])
}
A <- X[,1]
tmp<-svd(t(A),nu=1,nv=Ntr)
U <- tmp$u
S <- tmp$d
V <- tmp$v
Sinv <- solve(S)
S <- c(S,rep(0,Ntr-1))
Sinv <- rbind(Sinv,array(0,c(Ntr-1,1)))
Ainv <- V%*%Sinv%*%t(U)
mu[1,] <-  t(Ainv)%*%G
# Residuals
M[1,] <- mu[1,]
summary(X%*%M - Y)
colMeans(mu)
tr_set <- data.frame(c(roi[,1],ids),c(roi[,2],rep(1,Ntr)))
names(tr_set) <- c("pix_id","class_id")
rm(roi)
# Totals of pixels in training set
table(tr_set$class_id)
## Estimate covariance of mistletoe class=============
Cov[1,,] <- Cov[6,,] / 4
Cinv[1,,] <- solve(Cov[1,,])
# Display endmembers (like ENVI)
windows()
k<-1
plot(1:Nb,mu[k,],type="p",xlab="Band",ylab="DN",col=Class_legend$colour[k],pc
h=19,ylim=c(0,max(mu)))
lines(1:Nb,mu[k,],col=Class_legend$colour[k],lty=2)
for(k in 2:Ncl)
{
        points(1:Nb,mu[k,],col=Class_legend$colour[k],pch=19)
        lines(1:Nb,mu[k,],col=Class_legend$colour[k],lty=2)
}
# Display
G <- D@data[ids,]
Y <- array(data.matrix(G),dim(G))
k <- 3
l <- 4
#for(k in 1:(Nb-1))
#for(l in (k+1):Nb)
{
        xr <- range(mu[,k]) * c(0.5,1.2)
        yr <- range(mu[,l]) * c(0.5,1.2)
```

```
        windows()
        plot(Y[,k],Y[,l],pch=1,xlim=xr,ylim=yr,xlab=paste("band
",k,sep=""),ylab=paste("band ",l,sep=""),cex=3*A)

#       points(y[,k],y[,l],cex=0.2,pch=16)
                points(mu[,k],mu[,l],col=Class_legend$colour,pch=19,cex=2)
        text(mu[,k],mu[,l],col=Class_legend$colour,labels=Class_legend$name,po
s=4)
}
## Compute class separability=========================
TD  <- array(NA,c(Ncl,Ncl))
I0 <- array(0,c(Nb,Nb))
diag(I0) <- 1
for(k in 1:Ncl)
for(l in 1:Ncl)
{
        if(k!=l)
        {
                        TD[k,l] <- 2*(1-exp(-Div[k,l]/8))
                                        }
}
diag(TD) <- 0
print(TD)
# Contingency analysis ================================
nt <- nrow(tr_set)
P <- array(NA,c(nt,Ncl))
y <- D@data[tr_set$pix_id,1:Nb]
for(k in (1:Ncl))
{
        dy <- t(t(y)-mu[k,])
        temp <- 0.5*rowSums(dy * (t(Cinv[k,,] %*% t(dy))))
        temp <- temp + 0.5*log(abs(det(Cov[k,,])))
        P[,k] <- temp
}
tmp <- max(P,na.rm=TRUE)
ind <- which(is.na(P))
P[ind] <- tmp
tr_set$mlc <- max.col(-P)
CM <- array(0, c(Ncl,Ncl))
for(k in 1:Ncl)
for(l in 1:Ncl)
CM[k,l] <- sum((tr_set$mlc==k)&(tr_set$class_id==l))
# Contingency analysis: confusion matrix
row.names(CM)<- Class_legend$name
dimnames(CM)[[2]]<- Class_legend$name
CM
# Overall accuracy
OA <- sum(diag(CM))/sum(CM)
#In %
OA*100
# Apply MLC ================================
```

```
MLC <- Dsub
MLC@data <- data.frame(array(NA,nc))
names(MLC)<-"class_id"
P <- array(NA,c(nrow(MLC),Ncl))
tmp <- Dsub@data
y <- array(data.matrix(tmp),dim(tmp))
for(k in (1:Ncl))
{
        dy <- t(t(y)-mu[k,])
        temp <- 0.5*rowSums(dy * (t(Cinv[k,,] %*% t(dy))))
        P[,k] <- exp(-temp)/(((2*pi)^(Nb/2))*sqrt(abs(det(Cov[k,,]))))
}
MLC$class_id <- max.col(P)
# Convert distance P to probability
Prob <- P
Nprob <- Prob
# Convert FML to memberships
memb <- Prob
for(k in 1:nc)memb[k,] <- memb[k,]/sum(memb[k,])
FML <- Dsub
FML@data <- data.frame(memb)
for(k in 1:Ncl)
{
        windows()
        image(FML,attr=k,col=gray((0:255)/255),axes=TRUE)
        title(main=paste("Fuzzy ML: ",Class_legend$name[k],sep=""))
}
names(FML@data) <- Class_legend$name
## Define the starting image configuration (F), define the necessary functions for
the MRF and simulated annealing==================
frac <- array(0,c(nc,Ncl))
tmp <- Dsub@data[,]
#dc <- array(data.matrix(tmp),dim(tmp))
dc <- y
epsilon <- 1e-6
N0 <- min(Ncl,Nb+1)
d0 <- array(0,c(N0,N0))
mu_ext <- cbind(mu,rep(1,Ncl))
dc_ext <- cbind(dc,rep(1,nc))
#musvd<-svd(mu)
musvd<-svd(mu_ext)
u0 <- musvd$u
v0 <- musvd$v
d1 <- musvd$d
for(i in 1:N0)
{
        if(d1[i]>=epsilon) d0[i,i]<-1.0/d1[i]
}
#d0<-t(d0)
d0 <- t(v0%*%d0%*%t(u0))
frac <-  t(d0%*%t(dc_ext))
```

```
#residual
res<-array(0,c(nc,Nb))
sumfr<-array(0,nc)
for(i in 1:nc)
{
  res[i,] <-frac[i,]%*%mu-dc[i,]
  sumfr[i]<-sum(frac[i,])
}
LSU <- Dsub
LSU@data <- data.frame(frac)
names(LSU@data) <- Class_legend$name
#windows(title='Results of linear unmixing')
#Nrow <- round(sqrt(Ncl))
#par(mfrow=c(Nrow,round(Ncl/Nrow)))
#if(FALSE)
for(k in 1:Ncl)
{
        windows()
        image(LSU,attr=k, col=gray((0:255)/255),axes=TRUE)
        title(main = paste('Fraction of class ',Class_legend$name[k], sep=''))
}
sep=''))
# SRM stuff ==========================
# Scale factor
S <- 3
lambda <- 0.9
# SA parameters
T0      <- 0.0
Tupd    <- 0.9
# If you want to see progress of SA, ste TRUE. Note: the code runs slower.
ShowProgress <- TRUE
# Do you have reference image?
WithRef <- FALSE
# Display large images?
ShowLarge <- TRUE
# A constant to ensure positive likelihood energy
k<-1
logd0 <- 0.5 * log(abs(det(Cov[k,,])))
for(k in 2:Ncl)
{
 s0 <- 0.5*log(abs(det(Cov[k,,])))
 if(s0<logd0)logd0<-s0
}
Mf <- Mc*S
Nf <- Nc*S
nf <- Mf*Nf
# Here real window size is 2*WSize+1
#WSize<- S-1
WSize  <- 1
tmp <- Dsub@data
d <- array(data.matrix(tmp),dim(tmp))
```

```
f <- array(0,nf)
# SRM pixel size
psizef <- psize/S
#Which is the TL point?
bb <- bbox(Dsub)
SRMdata <- data.frame(f)
names(SRMdata) <- "class_id"
xyoffset <- c(bb[1,1],bb[2,1])
xyoffset <- xyoffset + 0.5*psizef*c(1,1)
srgrid <-
GridTopology(cellcentre.offset=xyoffset,cellsize=psizef,cells.dim=c(Mf,Nf))
SRM <- SpatialGridDataFrame(srgrid,SRMdata,proj_image)
#windows()
#image(D.image,red=nR,green=nG,blue=nB,axes=TRUE)
#title(main=paste("R:G:B=",nR,":",nG,":",nB,sep=""))
#points(coordinates(SRM))
# Neighbours: coordinates and weights======================
# Number (maximal) of pixel neighbours
Nmaxnb          <- (WSize*2+1)^2
Nns <- array(0,Mf*Nf)
Bns <- array(0,c(Mf*Nf,Nmaxnb))
Wns <- array(0,c(Mf*Nf,Nmaxnb))
for(pnf in 1:nf)
{
        j <- floor((pnf-1)/Mf)+1
        i <- pnf-(j-1)*Mf
   imin <- i - WSize
   imax <- i + WSize
   jmin <- j - WSize
   jmax <- j + WSize
   if(imin<1)  imin <-1
   if(imax>Mf) imax <-Mf
   if(jmin<1)  jmin <-1
   if(jmax>Nf) jmax <-Nf
        nxrange <- imin:imax
        nyrange <- jmin:jmax
        Nxdir <- length(nxrange)
        nxyrange <- cbind(nxrange,rep(nyrange,each=Nxdir))
        ndist <- nxyrange
        ndist[,1] <- ndist[,1]-i
        ndist[,2] <- ndist[,2]-j
        nrange <- nxyrange[,1]+(nxyrange[,2]-1)*Mf
        Nns[pnf] <- length(nrange)
        Bns[pnf,1:Nns[pnf]]<- nrange
        distnb <- sqrt(ndist[,1]^2+ndist[,2]^2)
        w <- which(distnb==0)
        distnb <- 1/distnb
        distnb[w] <- 0
        distnb <- distnb/sum(distnb)
        Wns[pnf,1:Nns[pnf]] <- distnb
}
```

```
# MRF and MCMC functions definition module================
I <- function(x,y){
        val <- 1
        if(x==y) val <- 0
        return(val)
}
Uprior <- function(pnf)
{
    W1 <- Wns[pnf,1:Nns[pnf]]
    f2 <- f[Bns[pnf,]]

         ind <- is.na(f2)
         W1[ind] <- 0
         f2[ind] <- 0
    f0 <- f2 - f[pnf]
    f0[f0!=0] <- 1
        # Now includes correction for counting each clique twice.
    val <-  0.5* sum(W1 * f0)
    return(val)
}
 Ulikelihood <- function(pnf)
{
        j <- ceiling(pnf/Mf)
        i <- pnf - (j-1)*Mf
        ic <- ceiling(i/S)
        jc <- ceiling(j/S)
        pnc <- ic + (jc-1)*Mc
        y0 <- y[pnc,]
        mm <- array(0, Nb)
        Cm <- array(0, c(Nb,Nb))
        # Update class fractions in the coarse pixel y
        nxrange <- ((ic-1)*S+1):(ic*S)
        nyrange <- ((jc-1)*S+1):(jc*S)
        Nxdir <- length(nxrange)
        nxyrange <- cbind(nxrange,rep(nyrange,each=Nxdir))
        nrange <- nxyrange[,1]+(nxyrange[,2]-1)*Mf
        f0 <- f[nrange]
        frac1 <- array(0,Ncl)
        for(k in 1:Ncl)
        {
                #frac1[k] <- sum(f0==k)/(S^2)
                frac1[k] <- sum(f0==k)/(length(nrange))
                Cm <- Cm + Cov[k,,]*frac1[k]
        }
        mm <- frac1%*%mu
        Cinv   <- solve(Cm)
        logdet <- 0.5 * log(abs(det(Cm))) - logd0
        val <-  0.5 * mahalanobis(y0, mm, Cinv, inverted=TRUE) + logdet
        return(val)
}
U <- function(pnf){
```

```
        val <- lambda * Uprior(pnf) + (1.0-lambda) * Ulikelihood(pnf)
        return(val)
}
TotalEnergy<-function()
{
        val <- 0
                for(pnf in 1:nf)
        {
                temp <- U(pnf)
                if(!is.na(temp))val <- val + temp
        }
        return(val/nf)
}
#   MCMC Energy optimisation ============================
Niter    <- 10000
#min_acc_thr <- 0.1*10^(-2)
min_acc_thr <- 0
MSE    <- array(0, 1)
Etotal <- array(0, 1)
Thist  <- array(0, 1)
T <- T0
# Initial SRM: downscale the hard MLC result
for(pnf in 1:nf)
{
        j <- ceiling(pnf/Mf)
        i <- pnf - (j-1)*Mf
        ic <- ceiling(i/S)
        jc <- ceiling(j/S)
        pnc <- ic + (jc-1)*Mc
        f[pnf] <- MLC@data[pnc,]
}
#f[] <- round(0.5+Ncl*runif(nf))
#f <- MLC$class_id
INSRM <- SRM
INSRM$class_id <- f
tmp <- array(0,Ncl)
for(k in 1:Ncl)tmp[k] <- sum(INSRM$class_id==k)
col_ind <- which(tmp>0)
image(INSRM, col=Class_legend$colour[col_ind],axes=TRUE)
title("Initial SRM")
stop_crit <- 0
E0       <- TotalEnergy()
for(iter in 1:Niter)
{
   upd_count <- 0
   for(pnf in 1:nf)
   {
                fu <- round(0.5 + runif(1, min=0, max=Ncl))
                ft <- f[pnf]
                if(!is.na(ft)&(fu!=ft))
                {
```

```
                        u1 <- U(pnf)
                        f[pnf] <- fu
                        u2 <- U(pnf)
                        u1 <- u2-u1
                        if(is.na(u1))
                        {
                                f[pnf] <- ft
                        }else
                        {
                                if(T!=0)
                                {
                                  u1 <- exp(-u1/T)
                                  xi <- runif(1, min=0, max=1)

                                  if(xi>u1)
                                  {
                                                f[pnf] <- ft
                                  }
                                  else upd_count<-upd_count+1
                                }
                                else
                                {
                                  if(u1>0)
                                  {
                                                f[pnf] <- ft
                                  }
                                  else upd_count<-upd_count+1
                                }
                        }
           }
        }
        Thist[iter]       <- T
#       if(WithRef)MSE[iter]     <-sum((Ref-f1)^2)/(nf)
        Etotal[iter]      <- TotalEnergy()
#       if(upd_count<=0)
        if(upd_count<=min_acc_thr*nf)
        {
                stop_crit <- stop_crit +1
        }else stop_crit <- 0
        if(stop_crit >=3) break
        T <- T * Tupd
#       T <- T0/log(2+iter)
        if(TRUE)
        {
                SRM$class_id <- f
                                tmp <- array(0,Ncl)
                for(k in 1:Ncl)tmp[k] <- sum(f==k)
                col_ind <- which(tmp>0)
                image(SRM,col=Class_legend$colour[col_ind],axes=TRUE)
                title(paste('Iter=',iter,sep=' '))
        }
```

```
}
SRM$class_id <- f
windows()
par(mfrow=c(2,2))
tmp <- array(0,Ncl)
for(k in 1:Ncl)tmp[k] <- sum(INSRM$class_id==k)
col_ind <- which(tmp>0)
image(INSRM, col=Class_legend$colour[col_ind],axes=TRUE)
title("Initial SRM")
if(WithRef)for(i in 1:nrefpol)
lines(VRef@polygons[[i]]@Polygons[[1]]@coords,col="red",lwd=2)
tmp <- array(0,Ncl)
for(k in 1:Ncl)tmp[k] <- sum(f==k)
col_ind <- which(tmp>0)
image(SRM,attr="class_id",col=Class_legend$colour[col_ind],axes=TRUE)
if(WithRef)for(i in 1:nrefpol)
lines(VRef@polygons[[i]]@Polygons[[1]]@coords,col="red",lwd=3)
title("Optimized SRM")
Etotal   <- Etotal[1:iter]
Thist    <- Thist[1:iter]
Etotal   <- c(E0,Etotal)
Thist    <- c(T0,Thist)
plot(0:iter, Thist, type = 'l', main = 'Temperature', xlab = 'Iteration', ylab = 'T')
plot(0:iter, Etotal, type = 'l', main = 'Energy minimisation', xlab = 'Iteration', ylab
= 'Etotal')
#draw_legend()
##evaluation of classification accuracy=================
# Reference proportions
tmp <- as.vector(t(pix_ids))
ind <- which(tmp!=0)
tmp2 <- tmp[ind]
tr_pixels <- tmp2
y <- as.vector(t(prop))
frac_ref <- y[ind]
# Read EM result (Mclust)
imagefn.in <- paste("EM_GE",".tif",sep="")
EM <- readGDAL(paste(Path_out,"/",imagefn.in,sep=""))
frac_em <- EM@data[tr_pixels,1]
# Read LSU result
imagefn.in <- paste("LSU_GG",".tif",sep="")
LSU <- readGDAL(paste(Path_out,"/",imagefn.in,sep=""))
tmp <- LSU@data
frac_lsu <- LSU@data[tr_pixels,1]
# Read FML result
imagefn.in <- paste("Likelihood_GG_class_mistletoe",".tif",sep="")
FML <- readGDAL(paste(Path_out,"/",imagefn.in,sep=""))
frac_fml <- FML@data[tr_pixels,1]
# Accuracy assessment
#FML
windows()
```

```
plot(frac_ref,frac_fml,xlim=c(0,1),ylim=c(0,1),xlab="Reference",ylab="FML
prediction")
lines(c(0,1),c(0,1))
rmse_fml <- sqrt(mean((frac_fml-frac_ref)^2))
cor_fml <- cor(frac_fml,frac_ref)
rmse_fml
cor_fml
# LSU
windows()
plot(frac_ref,frac_lsu,xlim=c(0,1),xlab="Reference",ylab="LSU prediction")
lines(c(0,1),c(0,1))
rmse_lsu <- sqrt(mean((frac_lsu-frac_ref)^2))
cor_lsu <- cor(frac_lsu,frac_ref)
rmse_lsu
cor_lsu
# EM
windows()
plot(frac_ref,frac_em,xlim=c(0,1),ylim=c(0,1),xlab="Reference",ylab="EM
prediction")
lines(c(0,1),c(0,1))
rmse_em <- sqrt(mean((frac_em-frac_ref)^2))
cor_em <- cor(frac_em,frac_ref)
rmse_em
cor_em
# The End====================================
```